https://doi.org/10.5194/egusphere-2026-3731
Preprint. Discussion started: 25 August 2026

Unified Aerosol Algorithm: New insights into the global aerosol system from the Ocean Color Instrument on NASA's PACE mission

Lorraine A. Remer[1], Hiren Jethva[2,3], Shana Mattoo[*,a] Omar Torres[3], Yingxi Rona Shi[1,3], Vinay Kayetha[4,3], Woogyung Vincent Kim [5,3], Jaehwa Lee[5,3], Robert C. Levy[3] and N. Christina Hsu[3]

[1] Goddard Earth Science, Technology And Research II (GESTARII), University of Maryland Baltimore County, Baltimore, 21228, USA
[2] Goddard Earth Science, Technology And Research II (GESTARII), Morgan State University, Baltimore, 21228, USA
[3] NASA Goddard Space Flight Center, Greenbelt, 20771, USA
[4] Science and Technology Corporation, Hampton, 23666, USA
[5] Earth System Science Interdisciplinary Center (ESSIC), University of Maryland College Park, College Park, 20740, USA
[*] Retired
[a] formerly of Science Systems and Applications, Inc., Lanham, 20706, USA

Correspondence to: Lorraine A. Remer (remer@umbc.edu)

Abstract. The launch of NASA's Plankton, Aerosols, Clouds, ocean Ecosystem (PACE) mission in 2024 with the Ocean Color Instrument (OCI) on board created new opportunity for characterizing aerosol properties from space. OCI observes Earth and its atmosphere across a broad spectral range in the reflective spectrum from the ultraviolet (UV) to the Short Wave InfraRed (SWIR). Heritage aerosol retrieval algorithms developed to accommodate radiometers measuring in the visible to SWIR wavelengths such as the MODerate resolution Imaging Spectroradiometer (MODIS) have been successful in characterizing aerosol optical depth (AOD) and indications of aerosol particle size but are less sensitive to aerosol particle absorption or aerosol layer height. Other heritage sensors measuring in the UV part of the spectrum such as the Total Ozone Mapping Spectrometer (TOMS) or the Ozone Monitoring Instrument (OMI) are sensitive to absorption and layer height but have insufficient information to constrain AOD in an aerosol retrieval. With OCI encompassing the entire spectral range of interest, the Dark Target and Deep Blue algorithms from the MODIS tradition and Near UV algorithm from the TOMS/OMI tradition are brought together, adapted for OCI and unified for retrievals of AOD, particle size parameter, aerosol absorption and aerosol layer height. Adaptations for OCI include adjustment for OCI sensor characteristics, modification of cloud and snow masking routines, production of the traditional UV Aerosol Index at unprecedented 1 km resolution, merging of the Dark Target and Deep Blue retrievals over land, extrapolation of spectral AOD retrieved in the visible range into the UV range, use of Oxygen-B bands for aerosol layer height, and retrieval of AOD above clouds that provides visualization of All Sky aerosol loading, Six months of retrievals have been compared with collocated AERONET AOD and single scattering albedo (SSA) resulting in a preliminary validation. AOD is biased high for shorter wavelengths, especially over ocean leading to asymmetrical error bounds for AOD. No similar bias is seen in the SSA retrievals which are exhibiting error bounds of ±0.04, at this stage. The results of the

https://doi.org/10.5194/egusphere-2026-3731
Preprint. Discussion started: 25 August 2026

OCI Unified Aerosol Algorithm are quantitative characterization of the global aerosol system over ocean, vegetated and barren surfaces, in clear skies and above clouds.

1 Introduction

Aerosols, small liquid or solid particles suspended in the atmosphere, are active players in Earth's energy balance and hydrological cycle (Szopa et al., 2021). When breathed into the lungs, these particles present a serious health hazard and have been identified as a leading risk factor of disease and shortened life expectancy (Cohen et al., 2017). Aerosols are global phenomena, produced in vast plumes that approach continental scales and which can be transported across oceans (Yu et al. 2008, 2012, 2013). The term "aerosol" is generic for a wide variety of substances having different chemical compositions, sizes, shapes, optical and hygroscopic properties, and depending on these properties, aerosols will have different effects on energy balance, hydrological cycle and health (Szopa et al., 2021). While in situ measurements from ground stations or aircraft may be the preferred means to obtain detailed characterization of aerosol composition and properties, in situ measurements are unable to characterize these particles on the global scale.

To determine aerosol loading and constrain some aerosol characteristics globally, we turn to satellite aerosol remote sensing. For decades satellite sensors have been observing the Earth system, including the atmosphere, in specific wavelength bands covering the part of the reflected solar and emitted terrestrial wavelength ranges (Torres and Remer, 2013). Algorithms applied to these measurements in specific bands have created many well-used data sets of quantitative aerosol characterization (Remer et al., 2020). The most pervasive of these products is aerosol optical depth (AOD) as a function of wavelength. AOD is a measure of aerosol loading in an optical sense and knowing aerosol loading is the fundamental parameter leading to estimates of aerosol effects in the energy budget, to identifying associations between aerosol amount and cloud properties, and to provide warning to populations when an air quality alert is forecasted. However, AOD by itself is only the first order parameter of interest. Other aerosol properties such as size, shape, absorption and layer height are necessary to reduce uncertainties in calculating aerosol effects on energy balance, interaction with clouds, health etc (Szopa et al., 2021). Satellite aerosol remote sensing retrievals have had less success in achieving these other parameters.

The first aerosol remote sensing algorithms made use of satellite observations in the visible (VIS) spectrum and this was expanded to the near-infrared (NIR) and shortwave-infrared (SWIR) spectral ranges as satellite sensor capabilities expanded to include those ranges. The AVHRR, MODIS and VIIRS aerosol products all stem from algorithms making use of these spectral ranges (Torres and Remer, 2013).

In parallel to the VIS-SWIR aerosol products, the near ultraviolet (nearUV or NUV) spectral range also developed during the 1990s. The Total Ozone Mapping Spectrometer (TOMS) and the Ozone Monitoring Instrument (OMI) aerosol products all derive from NUV retrievals (Herman et al., 1997; Torres et al., 2007). The UV spectral range is dominated by molecular scattering. Insertion of a layer of aerosol disturbs the signal expected by a pure molecular atmosphere, and it is this disturbance that is translated into an aerosol retrieval. The disturbance is registered by a difference in expected UV reflectance at top-of-atmosphere and also by the spectral slope of the UV reflectances (Torres and Remer, 2013). Thus, there are *two* pieces of information available to characterize aerosol in the UV. However, the retrieval is sensitive to *three* parameters: 1) the aerosol loading (AOD) 2) the absorption properties of the aerosol and 3) the height of the aerosol layer (Torres et al., 1998). While parameters (2) and (3) also play a role in the VIS-SWIR retrieval, the sensitivity is much less than the sensitivity of the loading (Remer et al., 2005). That is why we can assume values for (2) and (3) in the VIS-SWIR retrieval to make a robust retrieval of (1). However, in the UV (1), (2) and (3) are equally weighted. Assumptions of one of the three parameters will yield retrievals of the other two, but unfortunately that retrieval is plagued with higher-than-ideal uncertainty. It has been shown, however, that when aerosol layer height can be prescribed using either surface-based lidar observations (Torres et al., 2005) or satellite-borne lidar measurements (Jethva et al., 2014), accurate single scattering albedo can be derived from near UV satellite observations.

To reduce the uncertainty in the near UV retrieval, one additional piece of information is needed. If a sensor had a broader spectral range, from the near UV to the SWIR, then the VIS-SWIR range would provide sufficient information for a robust retrieval of spectral AOD. That information could be passed to the near UV retrieval, thereby constraining the aerosol loading

https://doi.org/10.5194/egusphere-2026-3731
Preprint. Discussion started: 25 August 2026

and allowing the near UV information to retrieve robust measures of aerosol absorption and aerosol layer height. Such an idea was tested in Satheesh et al. (2009, 2010) using collocated MODIS and OMI inputs. The result showed much improved aerosol layer height retrieval when compared to lidar measurements. No validation of aerosol absorption was possible. The method was never put into operational production, as MODIS and OMI were on separate platforms and involved in separate missions.

All of the above discussion refers to algorithms making use of multispectral radiance inputs. Another path to take for aerosol retrieval is to make use of hyperspectral techniques, specifically in the Oxygen absorption bands. This allows for retrieval of aerosol layer height (Xu et al., 2017, 2019).

The satellite measurement capability of combined NUV, VIS, and near IR radiances was achieved for the first time by the Earth Polychromatic Imaging Camera (EPIC) on the Deep Space Climate Observatory (DSCOVR) at the Lagrangian 1 (L1) point (Marshak et al., 2018). The availability of Oxygen-A and Oxygen-B channels along with near UV observations allowed for the first time the application of an algorithm that simultaneously retrieves NUV aerosol optical depth and single scattering albedo along with the aerosol layer height at a coarse 18 km resolution (Torres et al., 2025). A similar 3-parameter algorithm was applied to observations by the TROPOspheric Monitoring Instrument (TROPOMI) on the European Sentinel-5 Precursor satellite (Torres et al., 2020) at a 3.5 km x 5m resolution. The second-generation Cloud Aerosol Imager (CAI-2) sensor on the Greenhouse Observing Satellite (GOSAT-2) includes 0.339 µm (backward viewing) and 0.377 µm (forward viewing) near UV channels at 460 m spatial resolution. Although GOSAT-2/CAI-2 near-UV observations spatial resolution is unprecedented, their 40 deg. viewing configuration difference (Hashimoto and Shi, 2020) complicates the applicability of the heritage near-UV retrieval approach.

Today an opportunity exists to combine the information from a broad spectrum instrument that covers the range from 0.35 µm to 2.25 µm, allowing both the VIS-SWIR and near UV aerosol algorithms to combine into a single Unified Aerosol Algorithm (UAA). This instrument is the Ocean Color Instrument (OCI) flying on the Plankton, Aerosol, Clouds, ocean Ecosystem

https://doi.org/10.5194/egusphere-2026-3731
Preprint. Discussion started: 25 August 2026

satellite (Werdell et al., 2019). Also OCI's hyperspectral capability allows independent measures of aerosol layer height using Oxygen band techniques. The primary UAA products are aerosol single scattering albedo (SSA), which is a measure of aerosol absorption, and aerosol layer height (ALH), in addition to spectral AOD.

In this paper we will describe PACE and OCI in Section 2 and introduce the heritage algorithms that form the basis of UAA in Section 3. Section 4 outlines the flow of the UAA to show how all the pieces are aligned and fit together. Section 5 describes the creative innovations incorporated into UAA. In Section 6 we present examples of the algorithm run on on-orbit OCI inputs and present a preliminary validation. The results are discussed in Section 7. Appendix A provides a list and explanation of UAA's standard products.

2 PACE and OCI

NASA's Plankton, Aerosols, Clouds, ocean Ecosystems (PACE) mission was launched in February 2024 for the purpose of obtaining remote sensing observations of Earth's oceans and atmosphere with additional applications for terrestrial science (Werdell et al., 2019). PACE is in an ascending sun-synchronous polar orbit at 98° inclination, with an equator crossing time of 13:00 local time and an altitude of 676.5 km. The observatory carries three instruments: the Ocean Color Instrument (OCI), the Spectro-polarimeter for Planetary Exploration (SPEXone) and the HyperAngle Rainbow Polarimeter 2 (HARP2). SPEXone and HARP2 are multi-wavelength, multi-angle imaging polarimeters with capabilities well-suited to further PACE's mission for oceanic, atmospheric and terrestrial purposes.

OCI is a hyperspectral imaging radiometer with a cross-track swath of 2700 km and a nominal pixel spatial resolution of 1.2 km. To minimize the amount of ocean glint in the images, OCI performs a 19.9° along track tilt that occurs at the subsolar point on each orbit. The instrument is pointing aft in the Southern Hemisphere and fore in the Northern Hemisphere. This tilt means that OCI is never pointed nadir and that there will be missing useable data for an aerosol retrieval at the point when the instrument tilts. The place of missing data follows the sun, appearing exactly over the equator only at the solar equinoxes. In the spectral range of 0.34 μm to 0.895

https://doi.org/10.5194/egusphere-2026-3731
Preprint. Discussion started: 25 August 2026

μm, OCI measures in 0.005 μm bands of 0.0025 μm spectral steps. In addition to this hyperspectral measurement in the UV-VIS-NIR, OCI makes measurements in seven discrete bands covering the NIR-SWIR spectral range: 0.94 μm, 1.038 μm, 1.25 μm, 1.378 μm, 1.615 μm, 2.13 μm and 2.26 μm. It is this broad spectrum from 0.35 μm to 2.26 μm that makes OCI such an attractive instrument for aerosol retrievals because the information is there to apply VIS-SWIR retrievals to obtain spectral AOD and then constrain the near UV retrieval to obtain robust SSA and aerosol layer height (ALH). Additionally, the narrow band widths through the Oxygen B band will allow an independent retrieval of aerosol layer height.

The UAA uses the following bands: 0.354 μm, 0.388 μm, 0.412 μm, 0.49 μm, 0.55 μm, 0.67 μm, 0.6771 μm, 0.6871 μm, 0.87 μm, 1.25 μm, 1.378 μm, 1.615 μm and 2.26 μm. These values are obtained from a weighted average of the two closest OCI nominal bands based on the bands' Relative Spectral Response (RSR) functions. The exceptions are the 0.6771 μm and 0.6871 μm bands that fall within and adjacent to the Oxygen B band. These two bands are used at their native spectral resolution.

3 Heritage Algorithms

Three heritage algorithms provide the basis of the new UAA algorithm that is applied to OCI observations. Dark Target (DT) and Deep Blue (DB) come out of the MODIS/VIIRS heritage and make use of the VIS-SWIR wavelengths. Near UV represents the TOMS/OMI/TropOMI heritage and make use of the UV part of the OCI spectrum. Each of these algorithms have been well-documented in the published literature, beginning in the 1990s. We have provided short summaries of each, along with extensive references for further information in the Supplemental Material. Here we introduce a few concepts that are especially pertinent to the UAA algorithm

The UAA algorithm produces several established parameters relatively unchanged from the heritage algorithms. The spectral AOD over the VIS-SWIR range in the UAA output is derived exactly the same way as it is derived in the DT and DB algorithms (Levy et al., 2013; Hsu et al., 2013) with slight adjustments for OCI inputs. The Look Up Tables (LUTs) used in the UAA in the DT and DB subroutines are taken directly from those algorithm's configuration for VIIRS

https://doi.org/10.5194/egusphere-2026-3731
Preprint. Discussion started: 25 August 2026

wavelengths (Sawyer et al., 2020; Hsu et al. 2019) as will be explained in Section 5.1. Furthermore, the DT over ocean algorithm continues to output the fine mode weighting factor (η) (Remer et al., 2005) defined in the governing equation

$$\rho_\lambda^*(AOD) = \eta\rho_\lambda^{*f}(AOD) + (1-\eta)\rho_\lambda^{*c}(AOD) \quad (1)$$

Where $\rho^*_\lambda(AOD)$ represents the LUT top-of-atmosphere reflectance at wavelength, λ, for a particular AOD in the LUT, the *f* and *c* superscripts represent the fine mode and coarse mode, respectively, and η is the mode weighting factor. Reflectance without an *f* or *c* superscript represents the total reflectance that is compared with the satellite measurement. At the 0.55 µm wavelength only, the η mode weighting factor corresponds to the fraction of AOD in the fine mode (Remer et al., 2005). The η factor over oceans along with the spectral AOD (VIS – SWIR) over oceans and AOD (VIS) over land, unchanged from heritage algorithms, are some of UAA's primary products.

The NUV heritage algorithm makes use of the spectral contrast in the signal between two near-UV wavelengths after the removal of Rayleigh scattering effects following the Lambertian Equivalent Reflectivity (LER) approach adopted in the early 1990s (Herman et al., 1997). Since most of the signal in this residue parameter is attributed to the aerosol effects, it was termed as UV Aerosol Index (UVAI) and formulated as,

$$UVAI = -100\left[log\left(\frac{I_{sm}}{I_{lm}}\right) meas - log\left(\frac{I_{sc}}{I_{lc}}\right) calc\right] \quad (2)$$

Where, I_{sm} and I_{lm} are the measured TOA radiances at a shorter and longer wavelength, respectively, from the satellite sensor and Isc and Ilc are the calculated radiance following the LER approach with the longer wavelength as a reference (Herman et al., 1997; Torres et al., 1998). UVAI varies between slightly negative numbers, down to about -1, generally associated with small size non-absorbing aerosol types, around zero for most clouds, and positive values for UV-absorbing aerosol types. The UVAI magnitude in the presence of absorbing aerosols depends mainly on the aerosol optical depth (AOD), the height of the absorbing aerosol layer

https://doi.org/10.5194/egusphere-2026-3731
Preprint. Discussion started: 25 August 2026

(Torres et al., 1998), and slope of spectral aerosol absorption (Jethva and Torres, 2011). Therefore, UVAI is the fundamental parameter of the NUV heritage, and it is one of the primary outputs from the UAA. The main difference between the UAA and heritage versions of the UVAI is that the UAA offers a 1 km spatial resolution option of the UVAI that has never been previously produced. See Section 5.5 for more details. The other heritage NUV products include spectral AOD in the UV extrapolated from VIS, SSA, aerosol layer height (ALH), and AOD above clouds. These other parameters are produced in the UAA, leveraged from heritage principles, but they have been enhanced beyond heritage, as will be described in Section 5.

4 UAA structure and flow

The UAA algorithm takes the three heritage algorithms and combines them into a flow structure that ingests OCI data to produce aerosol parameters. The main purpose of the DT and DB heritage algorithms is to produce outputs of cloud-cleared spectral reflectances, AOD and η that the Near UV subroutine will ingest and use to constrain their heritage retrieval. These constraints allow for the near UV algorithm to proceed without the traditional uncertainty of three unknowns and only two pieces of information. Additionally, the Near UV algorithm benefits from DT and DB cloud masking traditions and uses η to choose between dust and smoke models in the Near UV LUTs.

Several innovations have been implemented into the UAA code. Over land the DT and DB retrievals are combined with new logic and the VIS-SWIR spectral AODs are extrapolated to the UV. The extrapolation is done internally in the DT ocean algorithm but is done externally over land using a Machine Learning model. The DT ocean algorithm has also implemented its own internal algorithm for retrieving SSA, as an alternative to the near UV method. Finally, UAA retrieves Above Cloud AOD when aerosol loading is strong, and has adopted an Oxygen band retrieval for aerosol layer height. These innovations and others are described in detail in Section 5.

Here we present the overall structure and flow of the UAA in Fig. 1. Subroutines arising from the near UV heritage are in light orange, DT heritage subroutines are in purple, DB heritage

https://doi.org/10.5194/egusphere-2026-3731
Preprint. Discussion started: 25 August 2026

subroutines are in dark blue and green indicates subroutines with no heritage that are unique to the UAA algorithms. The output is captured in light blue.

The UAA code reads in OCI reflectances at 0.005 µm resolution (0.0025 µm resolution for the Oxygen B band subroutine) and processes these hyperspectral bands to match the wavelength expectations of the LUTs of the three heritage traditions. Immediately the code calculates the UV Aerosol Index (UVAI). The UVAI requires no cloud masking and provides valuable first looks of aerosol events and climatology.

After the UVAI is calculated the subroutine diverges between over land and over ocean retrievals. This requires an ancillary land/ocean data base. If the retrieval is over ocean, the DT ocean subroutine is invoked. The subroutine requires nine spectral reflectances. Within the subroutine the DT ocean cloud mask (Martins et al., 2002; Remer et al., 2012) is applied and the heritage algorithm proceeds, but with a few modifications described in Section 5. The outputs from the DT ocean algorithm (AOD in the UV-SWIR, η and the cloud cleared reflectances) are made available to the near UV subroutine and also output in the final product. The DT ocean algorithm continues to perform an independent retrieval of SSA, shown in a green box in Fig. 1, and described in Section 5.2. The DT SSA is output in the final product.

If the retrieval will be over land both the DT and DB subroutines are invoked. Each proceeds as described above, with several modifications implemented that adapt the heritage code to the OCI configuration described in Section 5.1. Clouds are masked and both DT and DB output AOD in three visible wavelengths. Continuing over land, the AOD output from DT and DB are merged to produce a single value of AOD, labeled as UAA AOD in Fig. 1. The VIS UAA AODs and the cloud-cleared reflectances over land are passed to the near UV subroutine. The near UV subroutine also requires AOD in the UV. The UAA has implemented a Machine Learning model, shown in a green box in Fig. 1 and described in Section 5.4, to perform that extrapolation of AOD from VIS to UV over land.

Now the near UV algorithm has everything to perform its retrieval over both ocean and land. Specific changes of the near UV algorithm for the UAA are described in Section 5.5.

https://doi.org/10.5194/egusphere-2026-3731
Preprint. Discussion started: 25 August 2026

The UAA also includes a module for deriving AOD above clouds (Section 5.6) and another for Oxygen B (O_2B) band retrievals of aerosol layer height (Section 5.7) that resides outside of the main flow of the algorithm. This routine ingests OCI reflectances in two 0.0025 µm bands and uses this information to derive aerosol layer height, independently of the near UV subroutine.

https://doi.org/10.5194/egusphere-2026-3731
Preprint. Discussion started: 25 August 2026

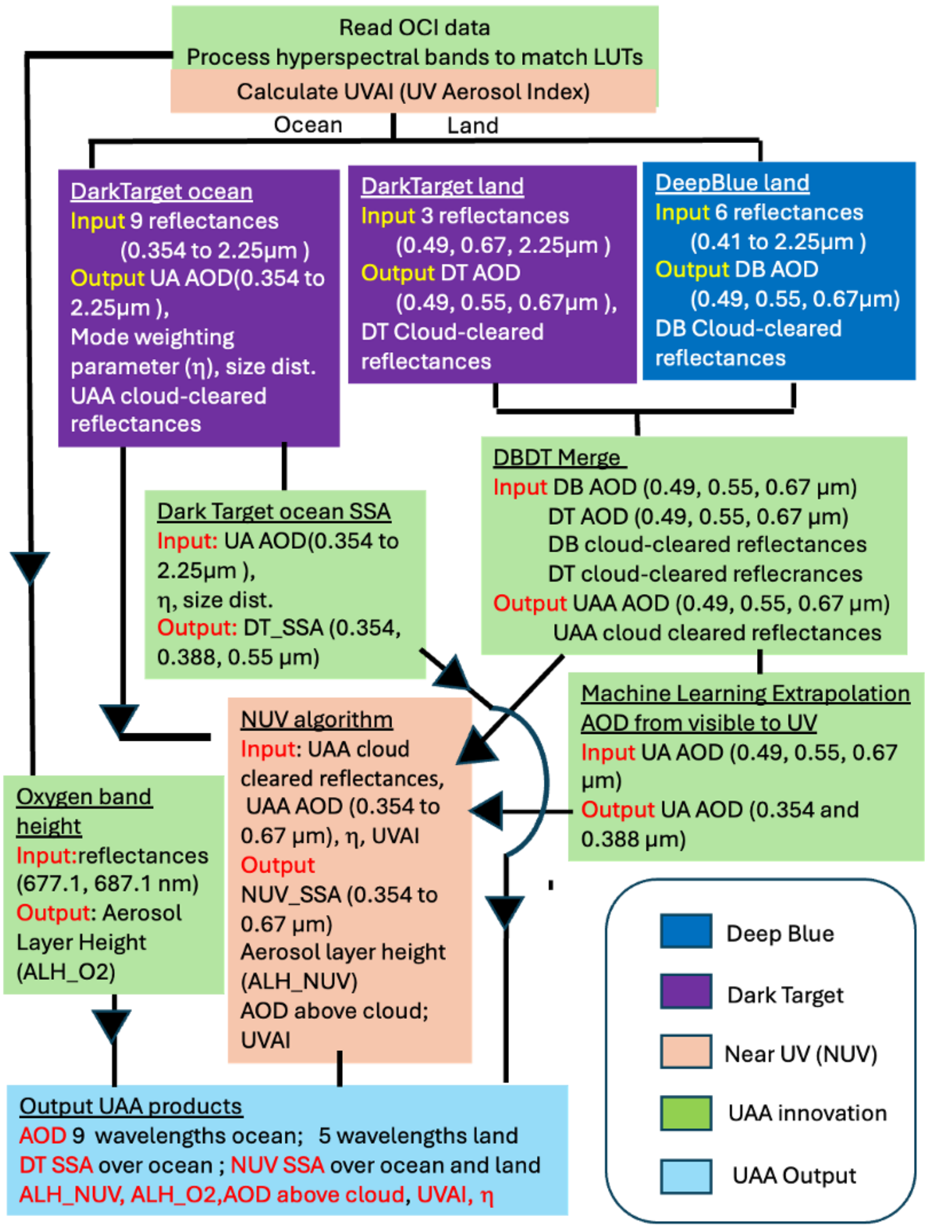

Figure 1. Flow chart showing over all structure of the UAA algorithm, from ingest of OCI data to output of UAA products. Heritage algorithms and specific UAA innovations are denoted by color code.

https://doi.org/10.5194/egusphere-2026-3731
Preprint. Discussion started: 25 August 2026

The final output of UAA include AOD in nine wavelengths over ocean and five wavelengths over land. Two independent spectral SSA products are produced, one originating from an internal DT retrieval and one output from the near UV subroutine. Both SSA products span the UV and VIS spectral range. There are two outputs of aerosol layer height, one derived using traditional near UV techniques and the other based on the O_2B bands. Other output products include the DT ocean mode weighting parameter (η) that is a robust physical measure of the fine mode fraction of the AOD at 0.55 μm (Remer et al., 2005), the AOD above clouds that can be combined with clear sky AOD to form a combined All Sky AOD product, and the venerable UVAI at two spatial resolutions. The full list of output parameters is tabulated and described in Appendix A.

5 UAA creative innovations

The UAA is based on three heritage algorithms but includes several creative innovations. Some of these innovations are to adapt heritage algorithms for OCI inputs or modify the algorithms to make use of the synergy of running the three algorithms together. Other innovations lead to new products, unique to the UAA.

5.1 Adapting DT and DB heritage to OCI sensor characteristics

New DT and DB LUTs have not been created for UAA. Rather than adjusting the LUTs, OCI bands are chosen and contiguous bands averaged to match the discrete wavelength bands used by heritage algorithms applied to VIIRS. Thus, the DT and DB LUTs used by the algorithms to process VIIRS inputs are used for UAA with no alteration.

The heritage DT algorithm inputs small chunks of 2-dimensional arrays of a sensor's native resolution and then uses that native resolution for cloud, snow, ice, glint, sediment and bright land surface masking. The masking is done by reading in an entire granule, one at a time. Then the algorithm calculates the mean reflectance of the remaining unmasked good pixels representative of the array (Remer et al., 2012). The mean reflectance of this array or retrieval

https://doi.org/10.5194/egusphere-2026-3731
Preprint. Discussion started: 25 August 2026

box moves forward in the retrieval to obtain aerosol products. The size of the array is sensor specific. The DB algorithm employs a different approach than the heritage DT algorithm. DB performs bad pixel masking (cloud, snow, etc.) at the sensor's native resolution and conducts retrievals at the pixel level. After obtaining retrievals at this native resolution, the algorithm then aggregates these pixel-level results to the reported spatial resolution.

For MODIS the DT algorithm used 20x20 arrays of 0.5 km native pixels because these matched the width of the MODIS scan mirror in the along-track direction. Here for OCI we do not need to consider width in pixels of a scan mirror as OCI uses a single telescope to make its cross-track scan (Meister et al., 2024). Instead, we choose a box size more comparable to DT VIIRS's finer resolution box and arrange OCI native pixels into retrieval boxes of 7 x 7 pixels of 1 km. All three heritage algorithms follow the DT tradition and organize their retrievals into these 7x7 pixel retrieval boxes. However, DB differs in that it conducts retrievals on each individual pixel of the native resolution observational data before aggregation. In addition to the UV Aerosol Index (UVAI) produced in the 7 x7 pixel retrieval box, the algorithm also produces the UVAI at OCI native resolution and makes the 1 km UVAI available in a separate data file.

The other modification needed by DT for OCI is to find substitutions for the missing thermal infrared wavelengths that all DT predecessor sensors offered but OCI does not. Thermal infrared (IR) wavelengths are used for both snow/ice and cloud masking. For snow masking, without a temperature sanity check, the land snow mask will erroneously identify snow pixels throughout the tropics. The problem is solved by using ancillary input reanalysis data (Global Modeling and Assimilation Office - GMAO) for skin temperature. For cloud masking by DT, the thermal IR test is a very minor contributor to the DT cloud mask that relies mostly on spatial variability using VIS channels, coupled with a 1.375 µm band for cirrus detection. The OCI UAA cloud mask over ocean and DT land retrievals simply drop the thermal IR test. This will introduce some isolated cloud contamination and mildly increase uncertainty in the product but should not be a driving factor in the overall uncertainty of the retrieval. The loss of the thermal IR wavelengths is more serious for DB, especially over bright deserts where heritage DT does not make a retrieval and where the DT cloud mask has never been applied or tested.

https://doi.org/10.5194/egusphere-2026-3731
Preprint. Discussion started: 25 August 2026

Despite this limitation, the adapted DB algorithm proceeds with aerosol retrievals without implementing a direct substitute for the thermal infrared (IR) tests. In the VIIRS DB algorithm, thermal IR measurements were also utilized for aerosol type classification, to enhance algorithm performance. Currently, no direct replacement for thermal IR observations exists within the OCI framework. Consequently, the decision was made to conduct retrievals without thermal IR capability, resulting in some sacrifice of algorithm performance. To minimize the degradation in algorithm performance, more stringent quality assurance tests were implemented in the retrieval process. The current implementation demonstrates adequate performance for operational applications, though future research may explore alternative methodologies to compensate for the absence of thermal IR information.

5.2 Extending DT for a SSA retrieval over ocean

The main innovation of the UAA is to constrain the AOD in the UV spectrum so that retrievals making use of that wavelength band are free to retrieve absorption parameters (SSA) and aerosol layer height (ALH). Over land, the AOD in the UV is extrapolated from retrievals made by the VIS-SWIR subroutines using a Machine Learning (ML) model that will be described in Section 5.4. Over ocean, the DT algorithm is modified to perform this extrapolation internally, as the DT over ocean algorithm is sufficiently sensitive to spectral extinction for an extrapolation to succeed. In fact, the extrapolation leads to a full DT aerosol retrieval using UV wavelengths that produce both a value of AOD and SSA in the UV over ocean. The Supplemental Material includes a section providing additional information on this internal retrieval including the parameters of the DT LUT over ocean with extension into the UV.

In Section 6 we demonstrate the DT SSA in two case studies, where it looks promising, but its quality is not consistent. Because currently we cannot fit reasonable error bounds on the DT SSA, we are treating the product as a diagnostic for the DT retrieval over ocean, and we are recommending users to not use the product for scientific purposes.

A more traditional method of obtaining SSA is made by directly adapting the NUV algorithm to OCI inputs and is described in Section 5.5. Validation for this NUV product is shown in Section 6.2.

https://doi.org/10.5194/egusphere-2026-3731
Preprint. Discussion started: 25 August 2026

5.3 DT/DB merge over land

Unifying the retrieval of AOD over land requires a merge of the DT and DB outputs. Previous attempts of creating a DT/DB merge were based on assumptions of each algorithm's strengths and weaknesses, using the Normalized Difference Vegetation Index (NDVI) as a guide (Sayer et al., 2014). The problem with this assumption is that it bases the decision only on surface cover and ignores all the other aspects of a retrieval. Local cloud cover, topography, aerosol types etc. may also contribute to aerosol retrieval uncertainty causing one retrieval to perform better than another.

For UAA we base the merge on actual validation statistics rather than surface cover type. DT and DB retrieved AOD at 0.55 µm from MODIS and VIIRS were collocated with AERONET Level 2 observations (Holben et al. 1998; Giles et al., 2019) using data from March 2012 through November 2020. The only data kept were situations when all three methods were reporting AOD, that is AERONET, DT and DB all reported an AOD simultaneously. The mean bias of both DT and DB against AERONET was calculated at each AERONET station. Then the difference in absolute bias of DT was subtracted from the absolute bias of DB and plotted for each AERONET station globally in Fig.2. Differences marked as blue indicate that DB has smaller absolute bias than DT, and the reverse is true for differences marked as red.

There are regional trends where each of the two land retrievals have historically shown smaller biases against AERONET. DB outperforms DT in the North American west, the African Sahel, the Iberian Peninsula and much of the Middle East and eastern Asia. Many but not all of these places are typified by drier vegetation and lower NDVI, as expected previously (Sayer et al., 2014). DT seems to hold an advantage in the North American east, northern South America, southern Africa, southeast Asia and much of Europe, some of which has higher NDVI, but not all. Given the map of Fig. 2, broad regional areas were drawn to identify which algorithm would take precedence in the UAA retrieval. Those regions are also shown in Fig. 2.

The logic of the merge is as follows:

https://doi.org/10.5194/egusphere-2026-3731
Preprint. Discussion started: 25 August 2026

- If neither DT nor DB produce a retrieval, all outputs in the green DBDT box of Fig. 2 are set to fill values.
- If DT produces a high quality retrieval and DB does not, then the UAA will move forward with the DT result.
- If DB produces a high quality retrieval and DT does not, then the UAA will move forward with the DB result.
- If both algorithms produce high quality retrievals, the UAA will use the AOD values from DT only in areas in which DT has precedence, as denoted by red rectangles in Fig.2 and defined here,

    a. -30 < Latitude < 45 AND -96 < Longitude <-58
    b. 45 < Latitude AND -20 < Longitude < 5
    c. 35 < Latitude AND 5 < Longitude < 36
    d. Latitude < 3 AND 5 < Longitude < 52
    e. -10 < Latitude < 30 AND 82 < Longitude < 112
    f. -10 < Latitude < 19 AND 112 < Longitude < 155
    e. -30 < Latitude < 15 AND 145 < Longitude < 160

Thus, in the default outside of these red boxes, if DB makes a retrieval, it will take precedence.

https://doi.org/10.5194/egusphere-2026-3731
Preprint. Discussion started: 25 August 2026

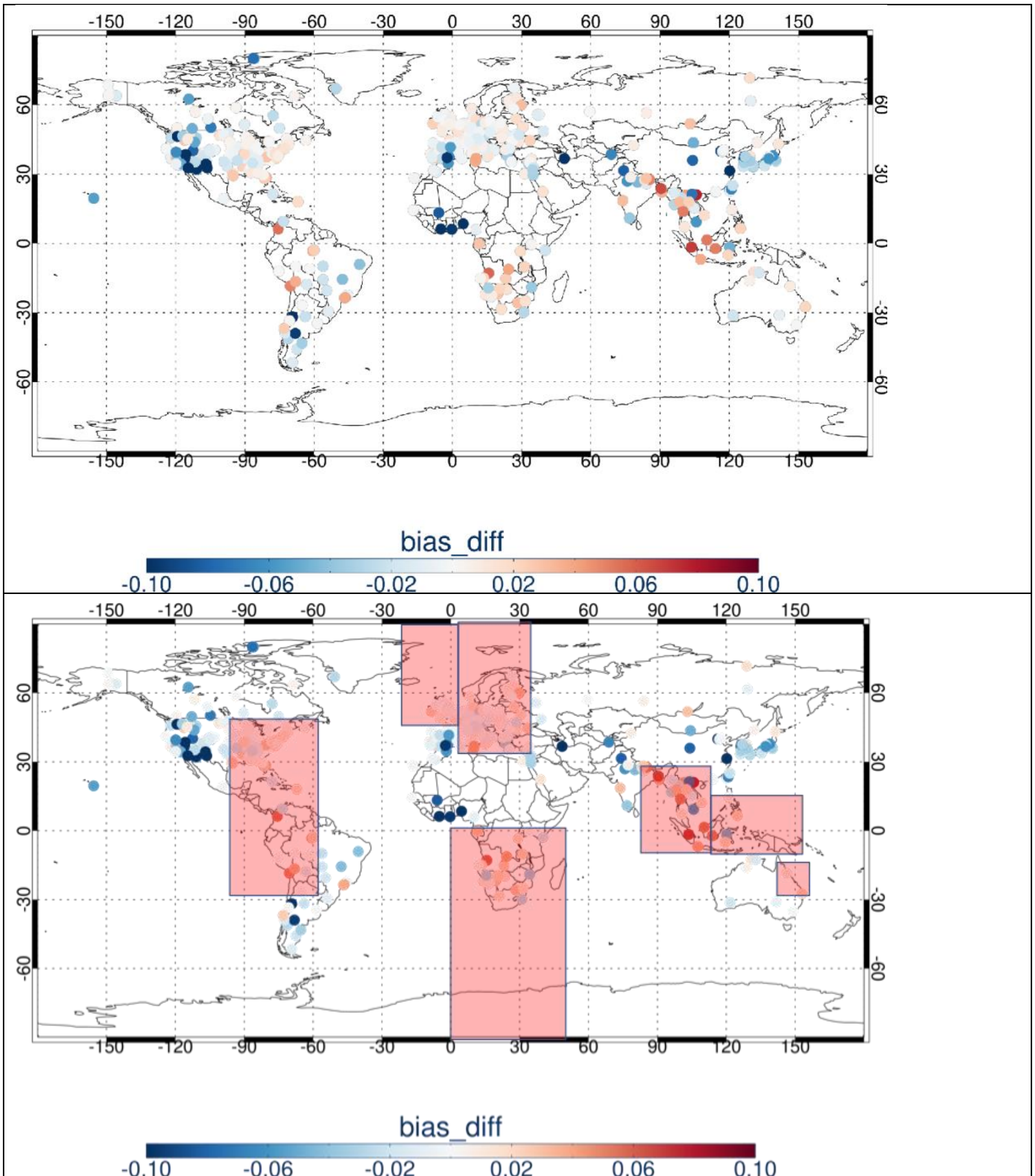

Figure 2. Mean absolute bias of AOD at 0.55 µm between Deep Blue (DB) retrieved values and AERONET observations minus the same but between Dark Target (DT) retrieved values and AERONET measurements. Negative values indicate that the DB bias is smaller than the DT bias, and vice versa for positive values. Thus, blue dots (top) identify AERONET stations where DB outperforms DT, and red dots identify where DT outperforms DB. Broad regions (bottom) colored red identify where DT will take precedence in the UAA.

5.4 Extrapolation of AOD to the UV over land

Over ocean, there is sufficient spectral information retrieved using the VIS-SWIR retrieval to extrapolate AOD into the UV spectral range, but over land the DB and DT retrievals are much more limited. The complexity of the land surface introduces too much uncertainty into the retrievals for robust spectral information to be recovered. Still, the UAA requires AOD in the UV spectral range to constrain the retrieval, making extrapolation a necessity.

The classical method of making a spectral AOD extrapolation is to use the Angstrom exponent. This assumes linearity in log-log space for the entire spectral range. Using AERONET AOD measurements at a long-term single location, Alta Floresta, we demonstrate the inadequacy of the linear extrapolation of the AOD into the UV. The extrapolations make use of three of AERONET's visible wavelengths that are similar to those retrieved by the Dark Target algorithm, nominally 0.44 µm, 0.50 µm and 0.675 µm. The extrapolated AOD at 0.38 µm is compared with AERONET's measured value. The results are depicted by the red and blue dots/regression lines in Fig. 3. The extrapolated values of UV AOD stray from the 1:1 line even for moderate AOD values and substantially overestimate AOD as aerosol loading increases.

The problem with Angstrom exponent extrapolations is that spectral AOD is not linear in log-log space (Eck et al., 1999). To deal with the nonlinearity, Satheesh et al. (2009), in a prototype to the UAA, used an empirical correction in the form of the weighted arithmetic difference between AOD at 0.47 and 0.87 µm. That correction was developed at a limited number of AERONET island stations and meant for over ocean retrievals. For the UAA extrapolation over land, we need a different approach, and because Eck et al., (1999) describe the spectral dependence of AOD as a quadratic in log-log space, we explored a quadratic extrapolation. The green points/regression line of Fig. 3 show the results of extrapolating into the UV from the visible using a quadratic fit. From that figure we see that the quadratic extrapolation matches the measurements much better than the linear ones, and if there were no other options we would have pursued a more universal quadratic fit from multiple AERONET stations worldwide. However, Machine Learning (ML) offers another option.

https://doi.org/10.5194/egusphere-2026-3731
Preprint. Discussion started: 25 August 2026

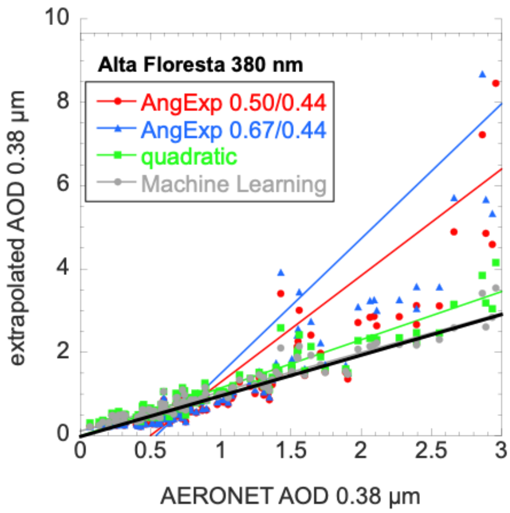

Figure 3. AOD at 0.38 µm extrapolated from AERONET observations of AOD at 0.44 µm, 0.50 µm and/or 0.675 µm compared with AERONET measurements of AOD at 0.38 µm at the Alta Floresta site covering the period 1993 through 2020. Each point represents the average of 1000 observations, after the data was sorted according to observations of AOD at 0.50 µm. Shown are estimates of AOD at 0.38 µm using two Angstrom Exponents(red and blue), each calculated from different pairs of visible wavelengths, the estimates from a quadratic fit (green) and estimates from a Machine Learning model (gray). The thick black solid line is the 1:1 line.

We develop a ML model using VIIRS and MODIS, DT and DB spectral AOD to predict collocated AERONET AOD in the UV bands. For MODIS, the collocated data from both Terra and Aqua from 2002 to 2015 are used. For VIIRS, the collocated data from 2016 to 2020 are used. Both over land and over ocean models are generated. However, because for the UAA we implement this extrapolation only over land, here we present and discuss only the over land model and validation. The ML model inputs three common wavelengths that DT, DB and UAA algorithms retrieve over land, namely 0.47, 0.55, 0.65 µm, along with month and geolocations. Other related parameters, such as viewing/illuminating geometries were tested but not used. A random forest model is selected to generate two independent over land models to predict AOD at 0.34 µm and 0.38 µm separately, while using the collocated AOD values from AERONET as "truth". The datasets are randomized to eliminate temporal dependency and then are randomly separated into training (80%) and testing (20%) data sets. Standard 10-fold evaluations are

https://doi.org/10.5194/egusphere-2026-3731
Preprint. Discussion started: 25 August 2026

performed to avoid overfitting. The fitted AOD accuracy are determined by the mean absolute bias (MAE) and root mean square error (RMSE). The overall testing error statistics show a MAE around 0.07 and a RMSE around 0.12 (Fig. 4), while the gray line in Fig. 3 illustrates the close fit to the 1:1 line in the Alta Floresta example. Additional case study evaluations and the tabulated statistics from the Alta Floresta analysis are given in the Supplemental Material.

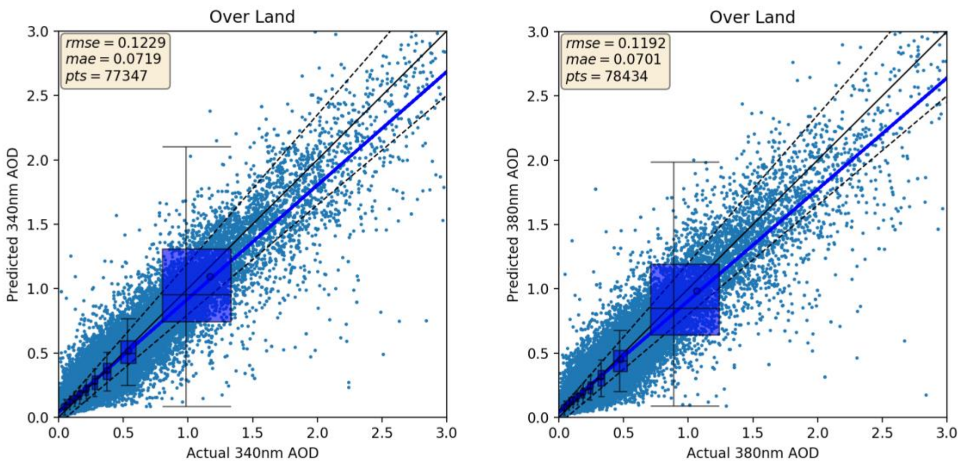

Figure 4: Scatterplots showing the AOD predicted by the Machine Learning (ML) model in the testing data set plotted against collocated AERONET equivalents for 0.34 µm (left) and 0.38 µm (right). Shown are the cloud of all points and whisker box plots constructed using 9 equal number bins from the data base sorted as a function of AERONET AOD. The one-to-one line is denoted by a solid black line and the dashed black lines are expected error defined as 0.05+15%. The linear regression calculated through the entire cloud of points is shown by the solid blue line. Statistics of the fit including Root Mean Square Error (rmse), Mean Absolute Error (mae) and the number of collocations in the plot (pts) are shown in the legend of each plot.

Based on the global comparisons with AERONET shown in Fig.4 and the comparison with other methods at Alta Floresta, the UAA will use the Machine Learning model to extrapolate AOD to the UV wavelengths for all over land retrievals.

https://doi.org/10.5194/egusphere-2026-3731
Preprint. Discussion started: 25 August 2026

5.5 UAA NUV retrieval

The UAA introduces several innovations to the heritage NUV retrieval method. Traditionally, the NUV algorithm has been applied to sensors with relatively large native pixel size (e.g., 13 km x 24 km for OMI). This has made cloud masking difficult and cloud contamination a constant threat. For OCI, clouds are identified at 1 km resolution using techniques long employed by the DT and DB algorithms (Remer et al., 2012). The NUV retrievals within UAA make use of the cloud-cleared pixels resulting from the DT and DB cloud mask and thus begin the traditional NUV retrieval with lower probability of cloud contamination.

As outlined in Section 4, the main advantage of the UAA algorithm is the passing of the AOD and particle size information from the DT and DB algorithms to the NUV algorithm. DT and DB retrieve spectral AOD using visible, near infrared and shortwave infrared measurements from OCI using their traditional algorithms with slight modifications. Then this AOD in the visible spectrum is extrapolated to the UV wavelengths needed by the NUV routine using a consistent internal aerosol model (over ocean) or a Machine Learning model (over land). Additionally, the DT and DB algorithms retrieve measures of particle size that can be used as a proxy for aerosol type, distinguishing between smoke and dust aerosols, necessary to direct the NUV algorithm to the proper LUT. The NUV algorithm then constrains the AOD in the UV to return values for aerosol layer height (ALH) and SSA necessary that match OCI's UV measurements using the correct LUT.

The other innovation applied here operationally for the first time is the extrapolation of the SSA retrieved for UV wavelengths back to the visible part of the spectrum using the analysis from Kayetha et al. (2022). Seasonal two-degree polynomials are constructed from the Kayetha et al. (2022) data base for different aerosol types and used to fill out the UAA SSA product at five wavelengths from 0.354 μm to 0.66 μm by pivoting these polynomials at the NUV retrieved SSA at 0.388 μm.

Another innovation resulting from the UAA applied to OCI is the relatively fine resolution UVAI parameter. The UAA aerosol products are derived and reported at a nominal 7 x 7 km^2 grid. Additionally, UAA provides UVAI at OCI's native pixel resolution of ~1.1 km. OCI is the first instrument to provide UVAI at such higher resolution on a daily scale, globally, rendering much

https://doi.org/10.5194/egusphere-2026-3731
Preprint. Discussion started: 25 August 2026

finer, detailed view of this valuable aerosol product. Fig. 5 displays three example maps of UVAI maps that were derived from OCI 0.354 – 0.388 µm observations at the 1.1 km native resolution. A close examination of these maps reveals strong positive values of UVAI, which indicates the presence of absorbing aerosols over or near biomass-burning sources in central and southern Africa, as well as in the Amazon and wildfire hotspots in Canada. Additionally, a detailed structure of clouds and their shadows can be observed over the South Atlantic Ocean. These high-resolution datasets should be further explored to gain more insight into the aerosol events in conjunction with, for example, other particulate ($PM_{2.5}$) and gaseous pollutants (NO_2, SO_2) for investigating correlative behavior between them.

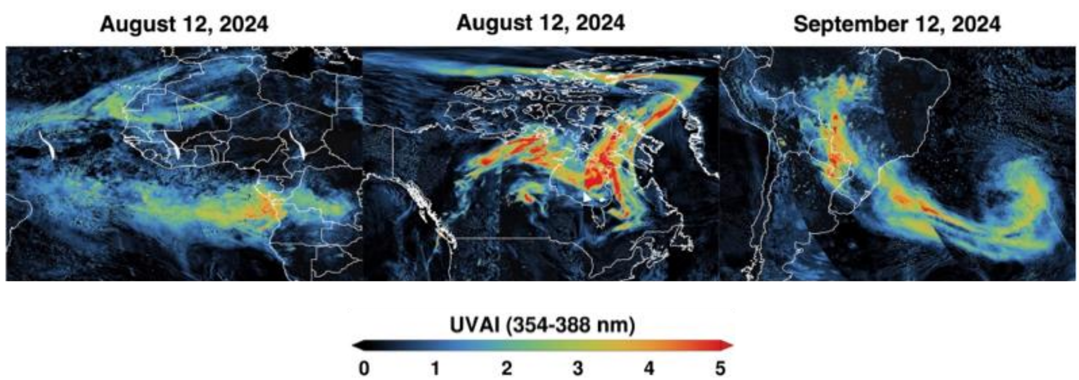

Figure 5. Regional maps of UVAI (0.354-0.388 µm) derived from OCI observations at a native spatial resolution of ~1.1 km for Aug 12 (left and center) and Sep 12 (right), 2024. Comparison of these retrievals with similar images from TropOMI is presented in the Supplemental Material.

5.6 AOD above clouds

Using the NUV concept to *qualitatively* detect above-cloud aerosols (ACA) has been explored since the introduction of the UVAI concept with the TOMS satellite (Herman et al., 1997; Hsu et al., 2003). However, the first *quantitative* ACA derivation was introduced using the OMI (Ozone Monitoring Instrument) near-UV observations (Torres et al., 2012), followed by the implementation of similar algorithms using MODIS visible observations (Jethva et al., 2013; Meyer et al., 2015; Sayer et al., 2016). The application of these retrieval approaches has provided region-specific and even global datasets of above-cloud aerosol optical depth (ACAOD), the latter from OMI (Jethva et al., 2018).

https://doi.org/10.5194/egusphere-2026-3731
Preprint. Discussion started: 25 August 2026

The near-UV technique uses the enhanced sensitivity of TOA observations to the spectral aerosol absorption over clouds to derive ACAOD and aerosol-corrected cloud optical depth (COD) in the 0.354-0.388 μm spectral region (Torres et al., 2012). Subsequently, a global algorithm was developed and applied to the long-term observation record of OMI (Jethva et al., 2018) to deduce a nearly two-decade-long ACAOD product. The OMI algorithm employs the same aerosol models representing particle size distribution of fine-mode carbonaceous smoke and mineral dust aerosols as OMI's NUV cloud-free algorithm. The modeled single-scattering albedo—the most critical assumption in ACAOD retrievals, was represented on a daily basis across 14 different regions. This was achieved by extracting region-specific UVAI-weighted cloud-free SSAs of the standard OMI NUV product. The aerosol type selection, whether smoke or dust, was based on daily AIRS carbon monoxide (CO) measurements (Torres et al., 2013). The ACAOD product derived from OMI was validated against direct airborne measurements from the High Spectral Resolution Lidar (HSRL-2) onboard the ER-2 aircraft during the ORACLES field campaign in the Southeastern Atlantic. This validation revealed a correlation of approximately 0.8, a minimal bias of less than 0.01, and a root mean square difference (RMSD) of about 0.1 (Jethva et al., 2018).

The availability of hyperspectral measurements from the OCI at 0.354 μm and 0.388 μm enables the direct adaptation of the OMI ACA algorithm for use with OCI observations. In this adaptation, most of the OMI algorithm remains unchanged, except for the two components: 1) the UAA version of the ACAOD algorithm makes use of the daily, regional dataset of above-cloud SSA extracted from the most recent retrieval database derived from the synergies of CALIOP lidar, and OMI-MODIS passive observations; the OMI-based above-cloud SSA dataset is used as a backup in case of no values found for a specific day and/or region, 2) we use the AIRS CO gridded monthly climatology for aerosol typing, instead of the daily AIRS CO dataset used in the OMI ACAOD algorithm. Additionally, the ACAOD algorithm within UAA benefits from an improved Dark Target cloud mask over land and ocean, which is derived from OCI's 1-km spatial resolution.

Figure 6 shows daily regional maps of the retrieved ACAOD (left panels) and composite AOD (above-cloud combined with cloud-free atmospheres) (right panels) at 0.388 μm derived from OCI 0.354-0.388 μm observations. Note the right column represents the All Sky AOD, the first such

https://doi.org/10.5194/egusphere-2026-3731
Preprint. Discussion started: 25 August 2026

product attainable from any operational satellite algorithm. One of the encouraging results, despite fundamental differences in the DT+DB vs. NUV ACAOD algorithms (i.e., aerosol models and inversion techniques), is the spatial continuity and the gradient along the transport pathways between the nearby cloud-free and above-cloud aerosol fields, especially for the smoke outflow in the Southeastern Atlantic Ocean. The remaining spatial discrepancies between the two sets of AODs can be attributed to two reasons: 1) intrinsic differences between the visible-based vs. NUV-based algorithm and their selection of aerosol models, and inversion approach, and 2) the cloud-free AODs correspond to the columnar aerosol loading from the surface to TOA, whereas ACAOD is a measure of the atmospheric aerosol column above the clouds. Therefore, above-cloud retrieval will miss the aerosol layer beneath the cloud, resulting in lower ACAODs.

https://doi.org/10.5194/egusphere-2026-3731
Preprint. Discussion started: 25 August 2026

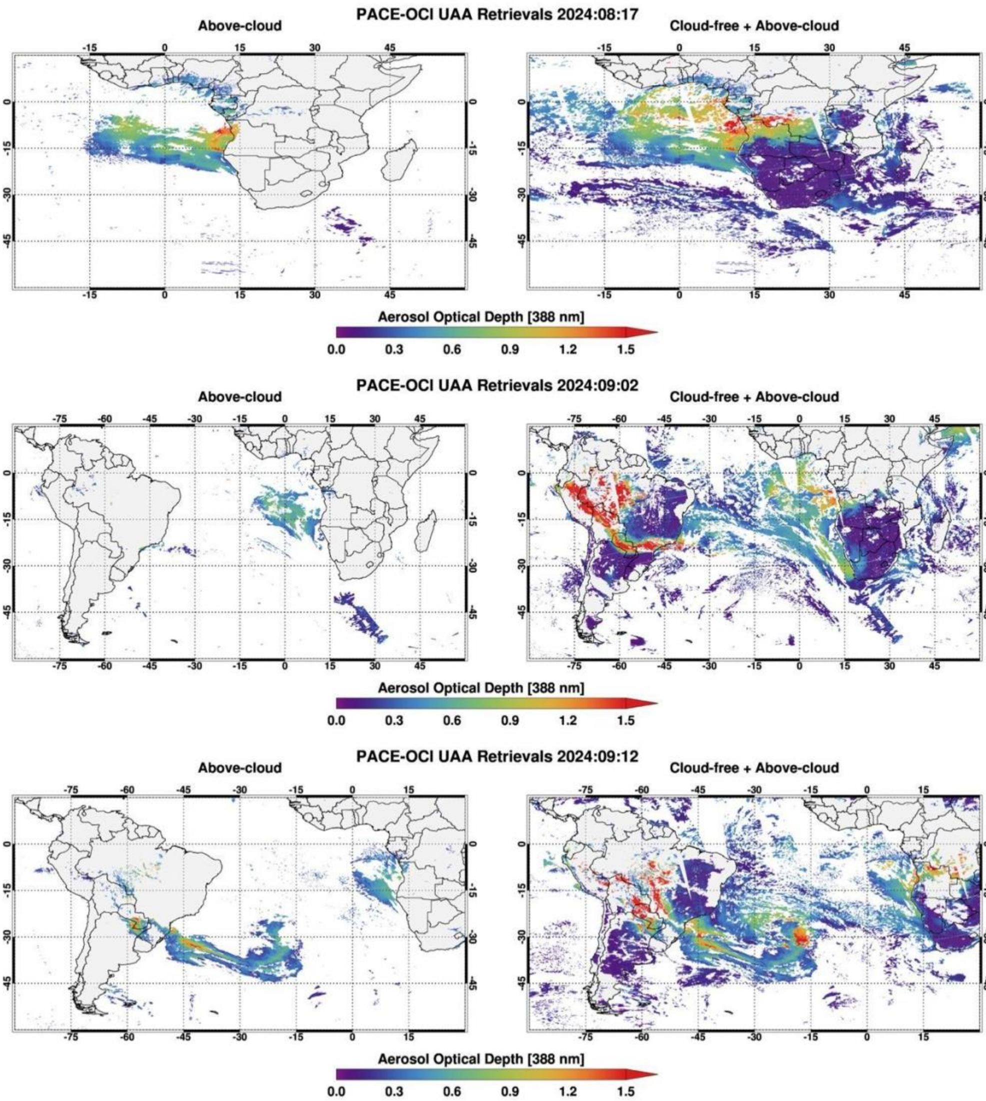

Figure 6. Case study examples of OCI-retrieved ACAOD (left panels) and composite, all-sky AOD (above-cloud combined with cloud-free) (right panels) at 0.388 µm over South/Southeastern Atlantic Ocean.

5.7 Oxygen-B band retrievals of aerosol layer height

The remote sensing technique that utilizes observations of the Oxygen-A and Oxygen-B (O_2-A and O_2-B) bands has been shown to be effective in retrieving the optical centroid of an aerosol

https://doi.org/10.5194/egusphere-2026-3731
Preprint. Discussion started: 25 August 2026

layer (Xu et al., 2017, 2019) that we will simply refer to as the aerosol layer height. To distinguish the layer height derived using Oxygen band techniques from that described in Section 5.5, we will refer to the NUV-derived as simply ALH or ALH_NUV, while the ALH derived from Oxygen bands will be denoted ALH_O2. While both bands (O_2-A and O_2-B) can be used to retrieve aerosol layer height over water surfaces, the larger surface albedo and associated uncertainties in the O_2-A (0.760-0.770 µm) wavelength range over land can present substantial challenges. In contrast, the O_2-B band is centered around the narrower wavelength range of 0.687-0.688 µm, where the land surface albedo is relatively lower. This makes the O_2-B band more suitable for ALH estimation over both land and water.

OCI's hyperspectral sampling at 0.0025 µm spectral interval around the O_2-B absorption lines offers a possibility to derive ALH_O2. The relative spectral response (RSR) function of OCI obtained from the instrument's characterization web portal (Meister, 2023) identifies two bands relevant to the O_2-B based ALH_O2 retrievals: one at 0.6771 µm, which is outside the absorption lines, and another at 0.6871 µm around the peak O_2-B absorption wavelengths. The corresponding RSR function for these two wavelength bands is shown in Fig. 7. The simulated TOA spectral reflectance at 0.001 µm resolution for an atmosphere with carbonaceous smoke aerosol layers placed at 2.5 km, 4.5 km, and 6.5 km is also shown in the same figure on the right-hand side of the y-axis. Detailed radiative transfer simulations at the O_2 hyperspectral absorption lines around 0.688 µm, along with O_2 absorption-free wavelengths outside this range, primarily around 0.677 µm, create a distinct contrast in the reflectance ratio (0.6871/0.6771). Figure 8 illustrates RT simulations comparing the reflectance ratio at 0.6871 µm to that at 0.6771 µm for an atmosphere characterized by two types of aerosols: a) carbonaceous particles and b) mineral dust. Aerosols are assumed to be vertically distributed following a quasi-Gaussian profile peaking at various altitudes. The particle size distribution and absorption properties of the carbonaceous and dust aerosol models used in this simulation were derived from a long-term, high-quality AERONET inversion dataset collected at the Mongu and Cape Verde sites, representing carbonaceous and dust aerosol types, respectively. The hyperspectral Top of Atmosphere (TOA) reflectance at 0.0001 µm spectral interval was convoluted using the OCI's RSR centered at 0.6771 µm and 0.6811 µm (See Fig. 7). This reflectance ratio (0.6871/0.6771) is notably sensitive to the altitude of the aerosol layer, where increasing height of aerosol layer is associated with increasing reflectance ratio

https://doi.org/10.5194/egusphere-2026-3731
Preprint. Discussion started: 25 August 2026

(0.6871/0.6771). This unambiguous signal results from the radiative attenuation of the incident solar light by aerosols, which restricts the penetration of light below the aerosol layer. Consequently, this reduces both the path length and the strength of the O_2-B absorption in the top-of-atmosphere (TOA) signal. We also see in Fig. 8 (third panel of top row) the importance of surface reflectance. Some combinations of aerosol absorption and surface reflectance nears the critical reflectance point (Fraser and Kaufman, 1985), thus rendering no sensitivity to aerosol loading. Yet, sensitivity to ALH remains.

The distinct sensitivity of the 0.6771-µm reflectance to AOD and reflectance ratio to the ALH forms the physical basis for simultaneously retrieving these two quantities. Hyperspectral, multidimensional aerosol look-up tables required for the inversion were created assuming carbonaceous smoke and mineral dust aerosol models derived from the long-term AERONET aerosol measurements taken at Mongu and Capo Verde sites, respectively. For cloud-free pixels aggregated to a 7 X 7 km^2 box, the two-channel O_2-B measurements of OCI are fitted to the aerosol LUT to retrieve ALH_O2 and AOD at the 0.6771 µm wavelength. The DT and DB components of UAA already retrieves AOD at 0.670 µm. It is anticipated that the O_2-B retrieved AOD at 0.6771 µm would carry larger uncertainty due to 1) the choice of a fixed value of SSA associated with chosen carbonaceous dust or dust model, and 2) the potential for situations near critical reflectance as demonstrated in Fig. 8. To avoid duplication and uncertainties, the AOD retrieved at 0.6771 µm is not currently reported in the output file in the UAA product.

https://doi.org/10.5194/egusphere-2026-3731
Preprint. Discussion started: 25 August 2026

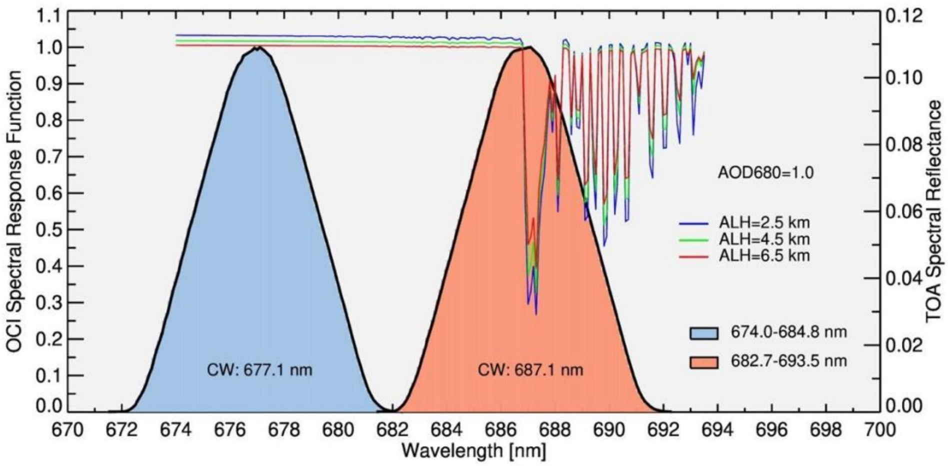

Figure 7 Normalized spectral response function of OCI around O_2-B absorption band (left y-axis). The simulated TOA spectral reflectance at 0.0001 µm for a carbonaceous smoke aerosol layer with AOD (0.677 µm) of 1.0 placed at 2.5 km, 4.5 km, and 6.5 km are shown on right-hand side y-axis.

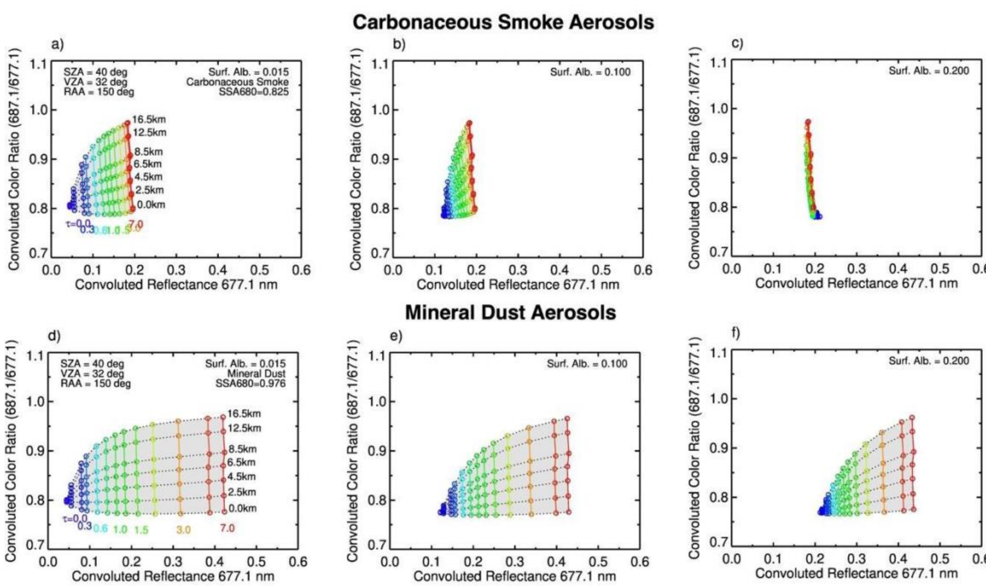

Figure 8. Radiative transfer simulations of color ratio (0.6871/0.6771 µm) vs. reflectance at 0.6771 µm of an assumed atmosphere with carbonaceous smoke (top panel) and mineral dust aerosols (bottom panel) for different combinations of AOD and ALH_O2. Here AOD is denoted as τ in the first panel of each row. Simulations are shown for a typical sun-satellite viewing geometry and for three different values of surface albedo of a) 0.015, b) 0.10, and c) 0.20.

https://doi.org/10.5194/egusphere-2026-3731
Preprint. Discussion started: 25 August 2026

6 UAA products and preliminary validation

The UAA algorithm produces products stored in two files. The main file gives products at the granule level organized in retrieval boxes of aggregated 7 x 7 native resolution pixels. The second file offers the UV Aerosol Index (UVAI) at OCI's native resolution, nominally at 1 km. A complete list of these products in the output files, their dimensions, and wavelengths are given in Appendix A.

6.1 Product demonstration

The first level of performance assessment is a demonstration of the products at the granule and global levels. This proves the algorithm is producing parameters that represent the aerosol system, as we know it to be.

The primary products at the granule level are shown for a wildfire smoke case and a dust case. The rgbs of these cases is shown in Fig. 9, and the products are illustrated for the smoke and dust cases in Figs. 10 and 11, respectively. The plots include points at AERONET stations (Holben et al., 1998; Giles et al., 2019) colored according to the same color bar for AOD and SSA. The UAA retrieved AOD at UV and visible, as well as NUV SSA, are very similar to what AERONET data show for both smoke and dust cases. Noteworthy is the All Sky AOD in the UV created as the combined results of clear sky AOD extrapolated from the DT or DB VIS-SWIR retrievals and the above cloud AOD (ACAOD). This product has never been produced operationally in this fashion. Also novel are SSA retrievals shown here for the primary UV wavelength but also available at 0.55 µm. The two methods for SSA retrieval are based on the same physical sensitivities and OCI inputs but make independent assumptions of aerosol model and other retrieval parameters. At this time we recommend using the NUV retrieved SSA and to treat the DT SSA as an unvalidated diagnostic parameter. We note some differences, but also very similar gradients when the two methods overlap in their spatial domain, especially for the smoke case. The similarity is a reassurance that the extrapolation to UV AOD over ocean for smoke is working within expectations. However, for the dust case, the DT SSA is overall higher than the NUV SSA, which suggests further analysis is required.

https://doi.org/10.5194/egusphere-2026-3731
Preprint. Discussion started: 25 August 2026

Two measures of aerosol layer height are shown in these figures. One is from the NUV subroutine, based on UV sensitivities, and the other results from the O_2-B retrieval. There is greater spatial variability in these products than in either AOD or SSA, which is not expected. We note that the NUV retrieval of ALH is strongly dependent on the entirety of the UAA retrieval, starting from the original retrieval of AOD from the heritage algorithms and extrapolation of the AOD to the UV, but the O_2-B retrieval is entirely independent of the bulk of the algorithm. Thus, it is reassuring to see the NUV and O_2-B retrievals of ALH agree so well where they both retrieve in the smoke case, producing physically realistic plume heights. The question with the smoke case is why does the NUV method retrieve in areas where O_2-B does not, and vice versa. The dust case is more difficult to understand where the two methods result in very different representations of the ALH field. When the two products diverge to this extent, caution should be exercised in using either one until validation can be established.

Figure 12 shows the global monthly mean maps of UAA products for the month of August 2024. Not shown is the ALH_O2 from the O_2-B subroutine, as that subroutine was too late to be included in the processing that produced the other variables. The AOD at 0.55 μm, UVAI and fine mode fraction (η) follow directly from heritage algorithms and present an aerosol global system just as we have come to expect from typical August conditions. New to UAA are the Above Cloud AOD, the SSA and the NUV ALH. Interestingly, while the DT and NUV SSA products appeared to agree well in the granule-level smoke case of Fig. 13, here we see that the NUV SSA product presents a global aerosol system significantly more absorbing than the DT equivalent over the global oceans where DT retrieves, more in line with the dust case of Fig. 14. Preliminary validation efforts with the NUV product suggest that the more absorbing world is the more accurate one, but comprehensive validation exercises are needed before we can make a recommendation between the two products.

This demonstration meets are expectations on the ability of the UAA to meet qualitative expectations of the global aerosol system.

https://doi.org/10.5194/egusphere-2026-3731
Preprint. Discussion started: 25 August 2026

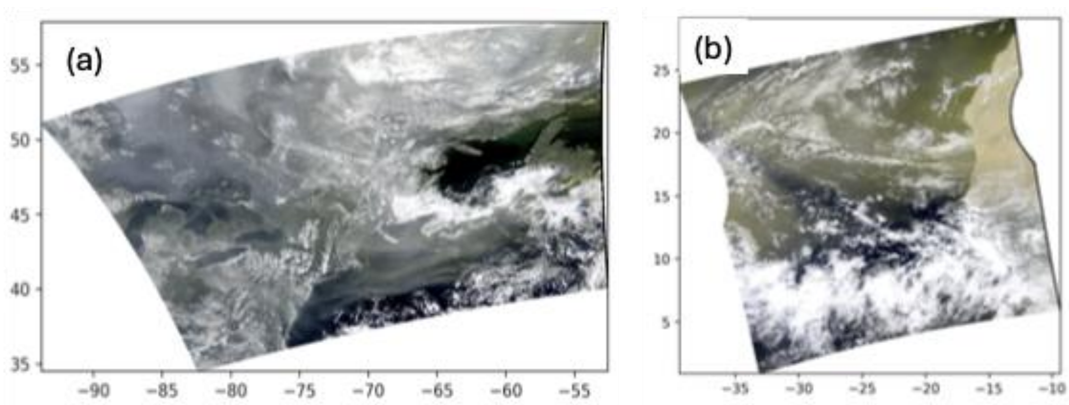

Figure 9. OCI true color (rgb) images of (a) long range transport of wildfire smoke from Canadian fires transported over the Canadian maritime provinces and the U.S. northeastern seaboard, 14 August 2024, and (b) a dust event that transported dust from northern Africa over the north tropical Atlantic on 15 July 2024.

https://doi.org/10.5194/egusphere-2026-3731
Preprint. Discussion started: 25 August 2026

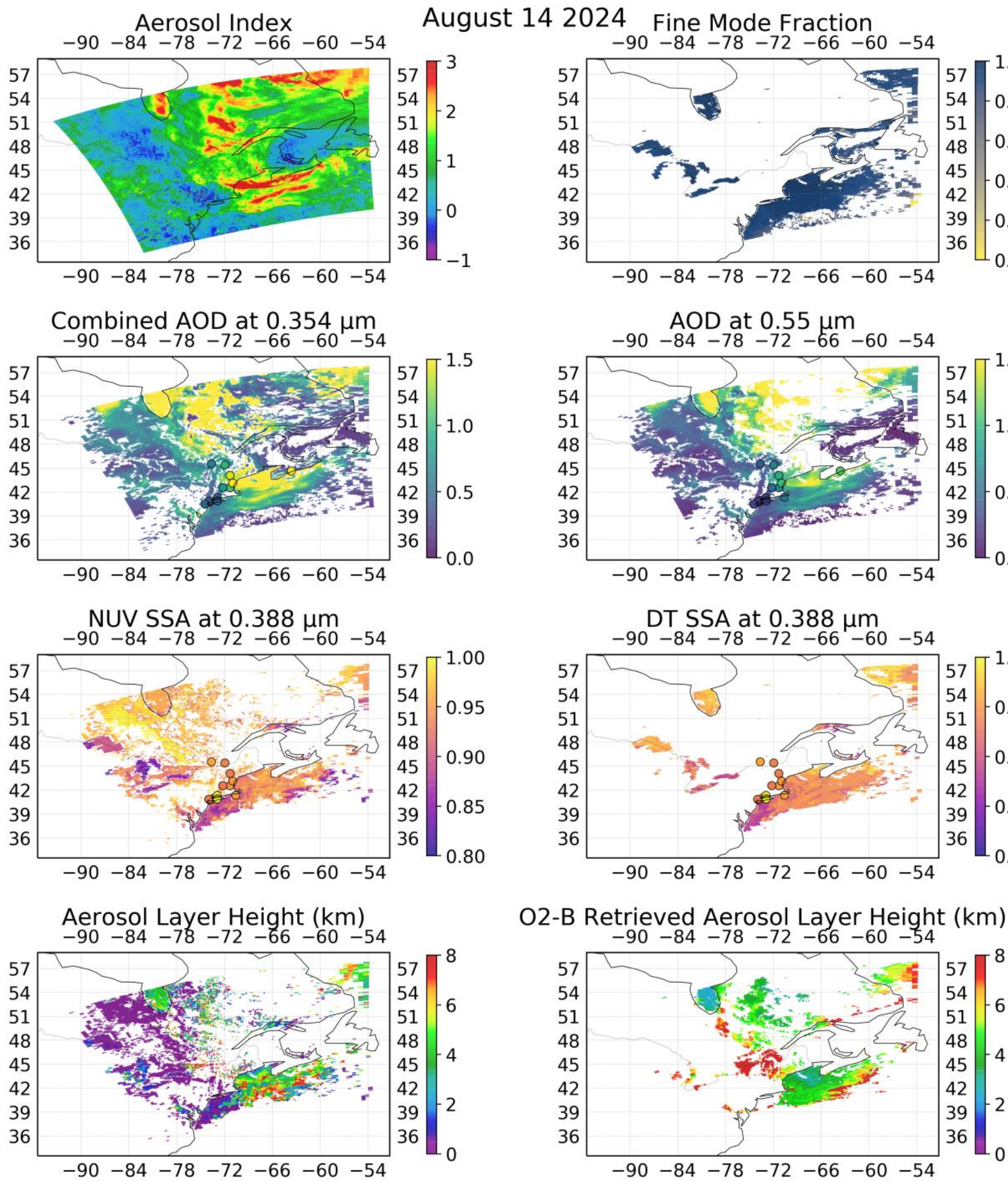

Figure 10. Eight products produced by the UAA from OCI measurements on 14 August 2024. The captured event is the long range transport of wildfire smoke from Canadian fires transported over the maritime provinces and the U.S. northeastern seaboard depicted in Fig. 9a. Shown and labeled are the UV Aerosol Index (UVAI), the fine mode fraction (η), the AOD at 0.354 µm combined from the cloud-free and above cloud aerosol routines, the clear-sky AOD at 0.55 µm, the SSA derived from the Near-UV (NUV) routine and the SSA

https://doi.org/10.5194/egusphere-2026-3731
Preprint. Discussion started: 25 August 2026

derived from the Dark Target routine, the aerosol layer height derived from the NUV routine (labeled simply as Aerosol Layer Height) and the ALH retrieved from the O_2-B method. Above cloud aerosol is only derived in the UV wavelengths and is not extrapolated to the visible. Dark Target SSA and fine mode fraction are only derived over ocean and large lakes. Small circles represent AERONET stations and the colors of those circles correspond to the same color as the UAA products. AERONET values are only available for AOD and SSA.

https://doi.org/10.5194/egusphere-2026-3731
Preprint. Discussion started: 25 August 2026

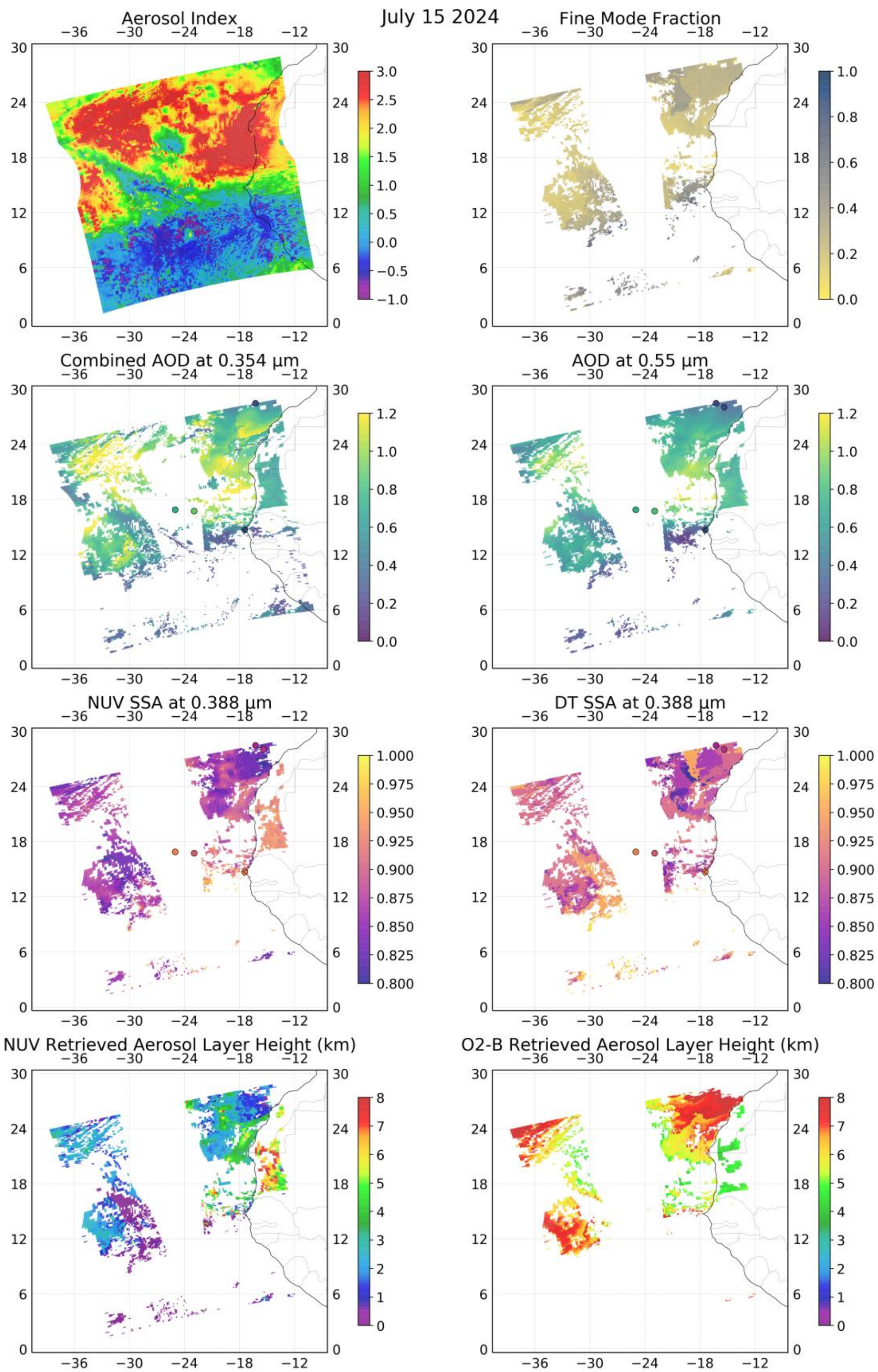

https://doi.org/10.5194/egusphere-2026-3731
Preprint. Discussion started: 25 August 2026

Figure 11 Same as Fig. 10 except for a dust event that transported dust from northern Africa over the north tropical Atlantic on 15 July 2024, shown in Fig. 9b. The empty space in the middle of the swath in most products is due to sun glint.

https://doi.org/10.5194/egusphere-2026-3731
Preprint. Discussion started: 25 August 2026

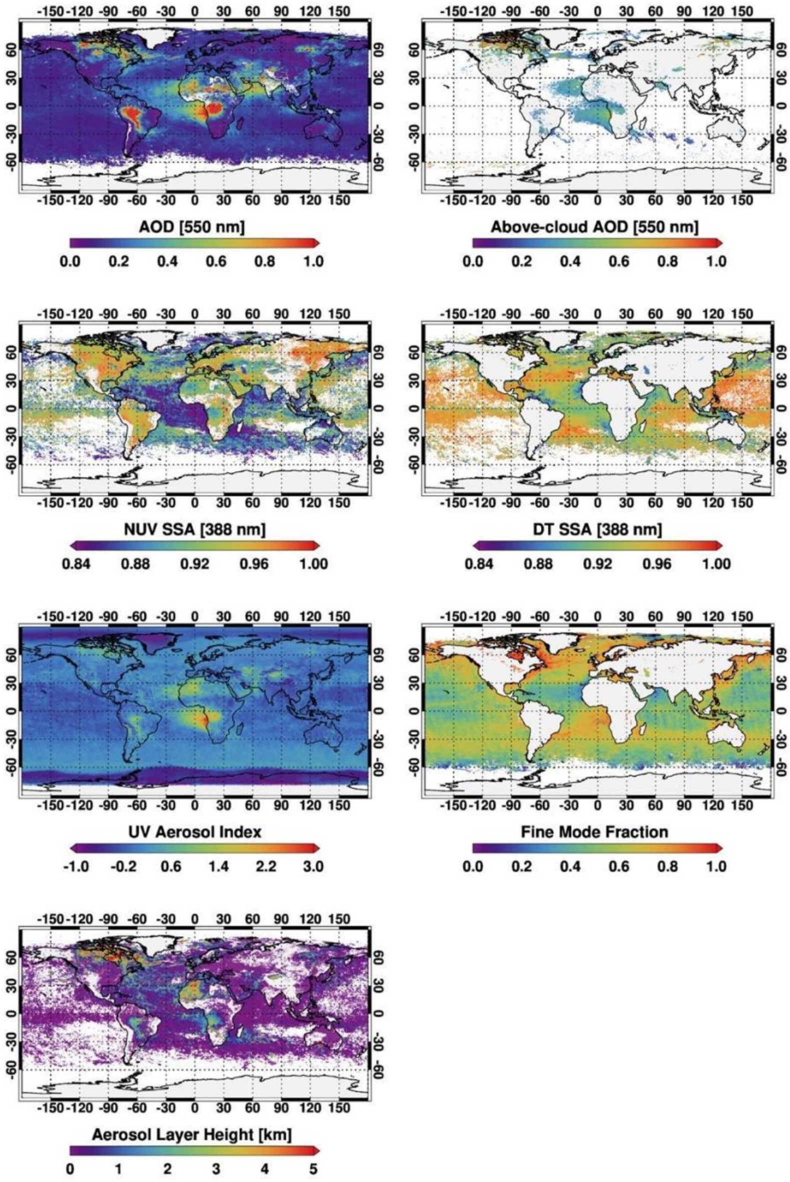

Figure 12. Monthly means of UAA products for the month of August 2024. Shown are AOD at 0.55 µm for the traditional clear sky and also above cloud aerosol, SSA at 0.388 µm from the NUV method, the UVAI, η – the fine mode fraction, and ALH from the NUV retrieval.

https://doi.org/10.5194/egusphere-2026-3731
Preprint. Discussion started: 25 August 2026

6.2 Preliminary validation

The AERONET network (Holben et al. 1998; Giles et al., 2019) provides the gold standard of ground truth for validation of satellite-derived aerosol products (Sayer et al., 2020). The spatio-temporal method devised originally by Ichoku et al. (2002), compares spatial statistics of the aerosol product retrieved from satellite with the temporal statistics of AERONET measurements or retrievals for collocated pairs of satellite and AERONET parameters. The collocation parameters that require definition for a validation include the spatial and temporal windows for each match-up, and filters to remove AERONET stations from the exercise when they are known to not represent the same aerosol retrieved from satellite in the defined spatial window.

UAA global products from April 2024 through September 2024 were collocated with AERONET stations using a spatial distance to the AERONET station of 0.25 latitude/longitude degrees or approximately a 50 km diameter circle centered on the AERONET station. For the AERONET temporal window we used 30 minutes of OCI overpass for AOD and 6 hours of overpass for SSA. Only Version 3 Level 2 AERONET parameters were included in the analysis. Ocean and land UAA retrievals are matched with AERONET and analyzed separately. AERONET stations contributing to the over ocean validation are island and coastal sites. Stations where the elevation of the AERONET station differs from the mean elevation of the AOD retrievals by more than 300 m are not included in the data set. This eliminates situations where the AERONET station is on a mountain top and not representative of the AOD retrievals in the 50 km circle. No Maritime Aerosol Network (MAN) data (Smirnov et al. 2009) are included here.

In Figs. 13 and 14 we see the ability of the UAA AOD retrieval to match AERONET values at UAA wavelengths. AERONET values are interpolated to UAA wavelengths using a polynomial fit in log-log space (Eck et al., 1999). Only five wavelengths are produced over land: 0.354, 0.388, 0.48, 0.55, 0.66 µm, and eight are produced over ocean: 0.354, 0.388, 0.55, 0.66, 0.87, 1.24, 1.61, 2.25 µm. Figure 14 shows only six of the eight ocean AODs. The collocation

https://doi.org/10.5194/egusphere-2026-3731
Preprint. Discussion started: 25 August 2026

statistics of Mean Bias, Root Mean Square Error (RMSE), slope of a regression line fit through the points and the number of collocations in the data set for that wavelength (N) are given for each wavelength in the AOD scatter plots.

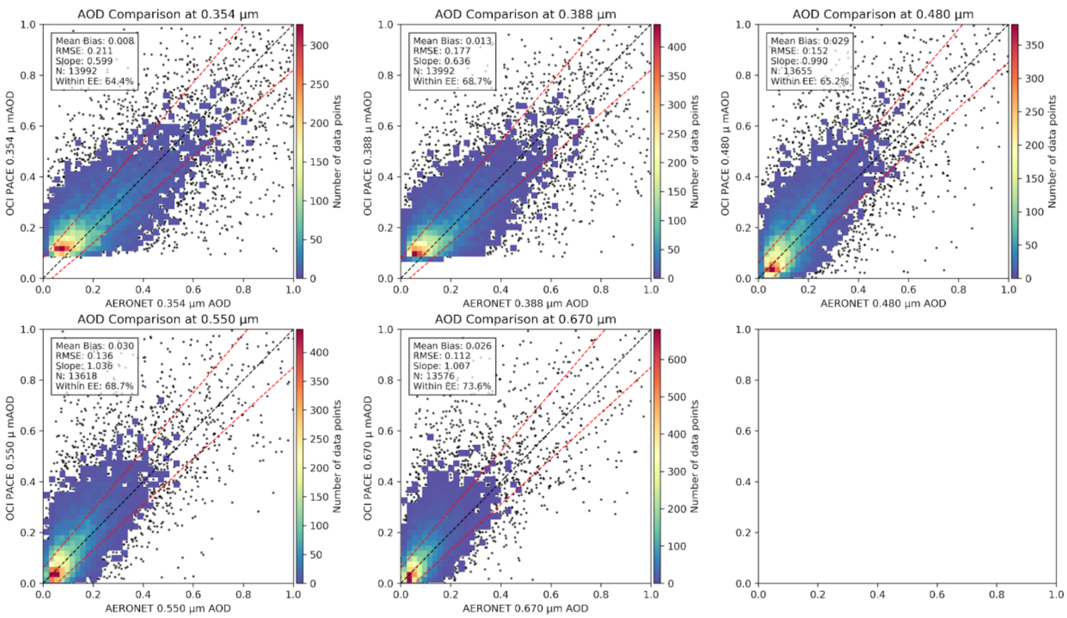

Figure 13. Density scatter plots of spectral AOD retrievals over land against collocated AERONET values. Shown are wavelengths retrieved over land: 0.354 µm, 0.388 µm, 0.48 µm 0.55 µm and 0.67 µm. Spatial collocations are defined as a 0.25 latitude-longitude degree radius circle around the AERONET site, and temporal collocations are ±30 minutes from PACE overpass. AERONET values are interpolated to OCI-retrieved values using a polynomial fit in log-log space. Collocation statistics for each wavelength are shown in each panel's legend. Data is calculated from a 6-month data set April to September 2024.

https://doi.org/10.5194/egusphere-2026-3731
Preprint. Discussion started: 25 August 2026

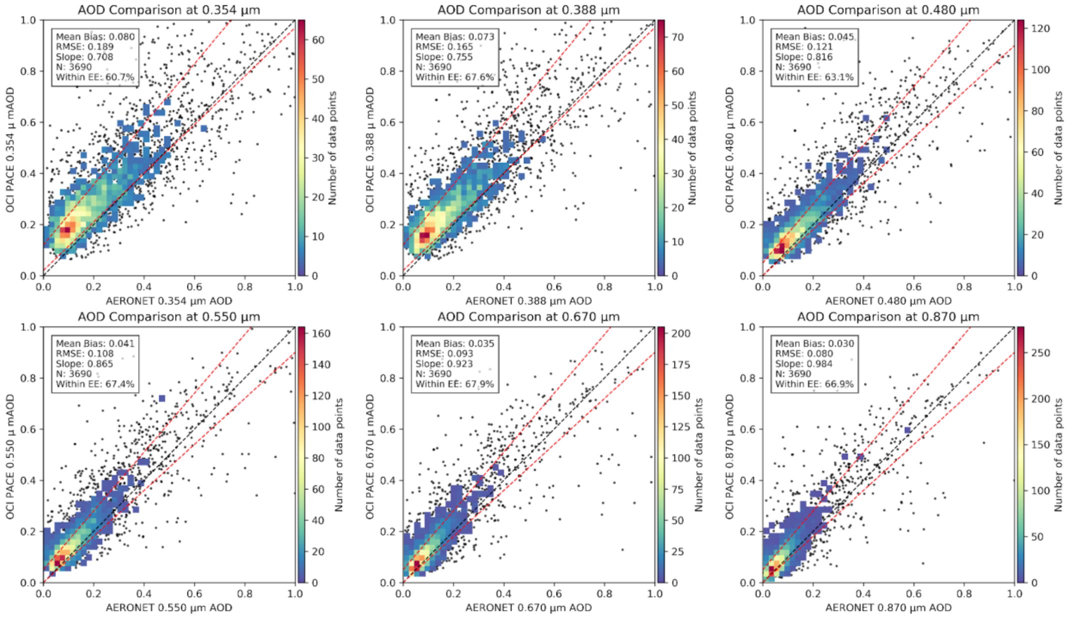

Figure 14. Same as Fig. 13, but for over ocean retrievals and including the values at 0.87 µm, retrieved over ocean but not land.

Both the land and ocean UAA retrievals show substantial skill at retrieving the spectral AOD. Table 1 shows UAA Mean Bias and RMSE falling between collocation statistics calculated from Aqua MODIS and SNPP VIIRS. MODIS and VIIRS values are taken from (Sawyer et al., 2020, 2025). In this preliminary validation exercise, we see that the UAA is producing results "in family" with heritage algorithms and sensors.

Table 1. Statistics of Mean Bias and Root Mean Square Error (RMSE) calculated from comparing retrieved AOD at 0.55 µm with collocated AERONET measurements for the UAA applied to OCI, the Dark Target algorithm applied to MODIS on Aqua (Sawyer et al., 2020) and the Dark Target algorithm applied to VIIRS on SNPP and NOAA-20 (Sawyer et al., 2025).

	Land	Ocean
Mean bias UAA OCI	0.030	0.041
Mean bias MODIS Aqua	0.008	0.026
Mean bias VIIRS SNPP	0.057	0.044
Mean bias VIIRS NOAA-20	-0.007	0.026
RMSE UAA OCI	0.136	0.108
RMSE MODIS Aqua	0.102	0.111
RMSE VIIRS SNPP	0.148	0.117
RMSE VIIRS NOAA-20	0.112	0.120

https://doi.org/10.5194/egusphere-2026-3731
Preprint. Discussion started: 25 August 2026

The collocation data set was used to determine the uncertainties of the UAA AOD product. Because of the relatively large mean bias that dominates for very low AODs, uncertainties are not symmetrical (Levy et al., 2013). At 0.55 µm, the bound on the error for the AOD retrieval can be described as

Land:

$$\text{Upper bound} = +0.06 + 0.15 * \text{AOD}$$

$$\text{Lower bound} = -0.05 - 0.10 * \text{AOD}$$

(3)

Ocean:

$$\text{Upper bound} = +0.05 + 0.15 * \text{AOD}$$

$$\text{Lower bound} = 0.00 - 0.10 * \text{AOD}$$

The asymmetrical bounds indicates that it is more likely for a retrieval to be positively biased than negative. These bounds establish “Expected Error” for the UAA results, and the dashed red lines in Figs. 13 and 14 represent these newly formed error bounds. “Expected” in this sense will set expectations going forward. In the preliminary validation shown here roughly 2/3 of retrievals at 0.55 µm fall within these error bounds. The error bounds derived using the 0.55 µm data will be applied to all visible, near IR and SWIR wavelengths.

The UV wavelengths that rely on extrapolation techniques described in Sections 5.2 and 5.4 are less accurate. In particular the positive mean bias is even more pronounced in the UV than in the visible. For the 0.388 µm wavelength the bound on the error for the AOD retrieval can be described as,

Land:

$$\text{Upper bound} = +0.08 + 0.15 * \text{AOD}$$

$$\text{Lower bound} = -0.03 - 0.15 * \text{AOD}$$

(4)

Ocean:

$$\text{Upper bound} = +0.12 + 0.18 * \text{AOD}$$

https://doi.org/10.5194/egusphere-2026-3731
Preprint. Discussion started: 25 August 2026

Lower bound = 0.02 – 0.05*AOD

As in the visible, these bounds establish "Expected Error" for the product moving forward. For simplicity, the same bounds determined for 0.388 µm are applied to 0.354 µm even though fewer than 2/3 of retrievals will fall within those bounds. The over land AODs in the UV fare better than the UV AODs over ocean. This suggests a move towards using a Machine Learning technique for ocean extrapolation may be preferrable to the internal method being used now. The uncertainties in the AOD extrapolation to the UV range will have direct consequences to the retrieval of SSA, both using the DT method and the NUV method.

In Fig.15, we show the match ups between UAA retrievals of NUV SSA against AERONET retrievals of the same for the one wavelength they have in common (0.44 µm). Shown are collocations using AERONET Levels 1.5 cloud-cleared near real time and 2.0, Quality Assured over all active sites for the period April through September 2024. The UAA NUV SSA is essentially unbiased in the aggregate when compared with AERONET, though moderately scattered. Root Mean Square Difference (RMSD) is ~0.04 and over ~67% of retrievals fall within ±0.04 error bars. This preliminary exercise suggests that our best estimate of error bars on the SSA is ±0.04, which is in the range of AERONET SSA uncertainty at this wavelength and AOD level. One note in these plots is the wide spatial variability of the SSA retrieval shown by the large vertical error bars for each collocated point. This spatial variability is under exploration.

https://doi.org/10.5194/egusphere-2026-3731
Preprint. Discussion started: 25 August 2026

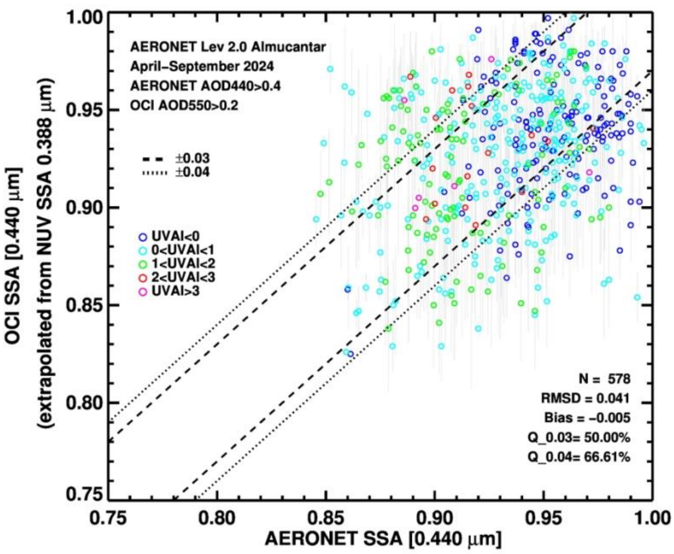

Figure 15. OCI UAA NUV retrieval of single scattering albedo (SSA) extrapolated to the 0.44 µm wavelength plotted against collocated AERONET Level 2 inversions (AOD440>0.4) of the same over globally distributed active sites during April through September 2024. Open circles represent the spatiotemporal means color-coded according to the coincident UVAI values. Gray vertical bars are the spatial standard deviation of all UAA retrievals within the 50 km diameter collocation circle surrounding the AERONET station. Dashed and dotted lines encompass all points ±0.03 and ±0.04 of the 1:1 line.

7.0 UAA Discussion and Conclusions

The UAA applied to OCI's broad reflective spectrum will introduce new perceptions of the global aerosol system. Adding to the well characterized global aerosol loading in the form of AOD, UAA is equipped with a vertical dimension to the retrievals and quantifying the absorption properties, as well as providing the venerable UVAI at unprecedented 1 km spatial resolution. The UAA is based on unifying heritage algorithms and reducing the traditional uncertainties of aerosol retrieval in the UV part of the spectrum introduced by the challenge of needing to derive three parameters: loading, absorption and height from only two pieces of information. The UAA uses the VIS-SWIR to constrain the loading for the NUV algorithm to produce the other two parameters. Additionally, the VIS-SWIR component of the UAA also does

https://doi.org/10.5194/egusphere-2026-3731
Preprint. Discussion started: 25 August 2026

the important work of cloud clearing and determining the size parameter to further reduce uncertainties in the retrievals of SSA and aerosol layer height.

Currently, UAA offers two flavors of SSA products: one following the tradition of the NUV heritage algorithm and one embedded in an extension of the traditional Dark Target (DT) retrieval. Both are based on the same physical phenomena, but they differ in assumptions of aerosol models and in retrieval methodology. The DT algorithm is applied only over oceans. The NUV algorithm is applied to all cloud-free conditions when AOD in the visible exceeds 0.2, except over snow and ice. The two products sometimes match well on a granule-by-granule basis, but when aggregated into global monthly means, the NUV produces a much darker, more absorbing aerosol than does the DT. Furthermore, the NUV SSA shows strong land/sea contrast on a monthly mean basis. In preliminary evaluation including collocations with AERONET when possible, it appears that the NUV SSA is closer to AERONET than the DT and that NUV's SSA over ocean retrieval is more accurate than its over land retrieval. Results are still very preliminary but current indications are that 67% of the NUV SSA retrievals at 0.44 µm fall within

$$\Delta SSA\_440 = \pm 0.04$$

of collocated AERONET retrievals. We note here that AERONET SSA retrievals themselves have uncertainties of ±0.03 and that the spatial variability of the UAA SSA product is high. Subsequent evaluation of both UAA SSA products, at multiple wavelengths is critical before we can recommend the DT SSA product and what accuracy to expect from it. Yet, these preliminary results are very encouraging.

The UAA also produces two measures of aerosol layer height (ALH). The first comes directly from the NUV algorithm after AOD is constrained and SSA is co-retrieved. This product is denoted as ALH. Thus, the AOD, SSA and ALH are internally consistent and are recommended to be used as a set of parameters for assimilation systems and calculations of aerosol radiative flux. The second measure of height is produced completely independently from the NUV or even the heritage VIS-SWIR routines, and this is ALH_O2 derived using O_2-B techniques. The O_2-B

https://doi.org/10.5194/egusphere-2026-3731
Preprint. Discussion started: 25 August 2026

was implemented into the UAA processing later than the other parameters and did not make the cut to be included in the processing that produced the global monthly mean maps. On a granule-by-granule basis, the NUV and O_2-B methods sometimes agree on ALH values but sometimes diverge wildly. Even in situations where the two methods agree when they retrieve in the same locations, nearby one will retrieve but the other method will not. True validation in the form of comparison to lidar or other measure of ALH will be needed to bring clarity to the ALH retrieval. The ultimate goal is to use the independent retrieval from O_2-B techniques to further constrain the NUV retrieval, allowing an even more robust retrieval of SSA. Furthermore, constraining the NUV algorithm with DT+DB AODs and ALH_O2 from O_2-B method would allow independent inversion of SSA at 0.354 µm and 0.388 µm, thereby spectral dependence of absorption-- an optical signature that can be used to infer the chemical/mineral composition of aerosols. However, this is something for the future upgrades when an opportunity strikes.

Two other innovations to mention are (1) the UAA's ability to produce an All Sky AOD by combining the traditional Clear Sky value on the same maps with the new Above Cloud AOD and (2) the 1 km UVAI product.

At this point, evaluation of the algorithm's products has been minimal and the results of that evaluation presented here are preliminary. Only six months of data have been examined. With this preliminary evaluation, we see that the heritage AOD in the VIS-SWIR, UVAI, and η (fine mode fraction) are meeting expectations based on more than 20 years of experience. The AOD product falls closer to VIIRS heritage results than to MODIS and retains a strong positive bias yielding asymmetrical error bounds. Throughout the VIS-SWIR bands 2/3 of AOD retrievals will fall within the bounds described by Eq. 3.

We are still forming expectations for the new products. Almost two thirds of the new extrapolated AOD at 0.388 µm over land appears to match AERONET to within the bounds set by Eq.4 on a global basis. The substantial high bias in the UV AOD is causing the NUV SSA to be systematically too high in some regions such as Africa. This bias contributes to the sharp land/sea contrast seen in Fig.12. Preliminary indications are that the aerosol should be more

https://doi.org/10.5194/egusphere-2026-3731
Preprint. Discussion started: 25 August 2026

absorbing with lower SSA and closer to the values of the surrounding oceans. The extrapolated AOD at 0.354 µm over land is more uncertain than at 0.388 µm.

Over ocean, the extrapolation is less certain with the AOD at 0.388 µm creating an even larger positive bias against AERONET of 0.073. The positive bias will cascade through retrievals of SSA by the DT method and through retrievals of SSA and ALH using the NUV method. Above all else, this extrapolation over ocean and the resulting consequence to other parameters requires further scrutiny.

Our final observation, implied by the above analysis is that OCI, the instrument, performed well during its first half year of observations. The v3 calibration coefficients used to produce the OCI radiances used by the UAA in this analysis required no additional corrections or adjustments to produce the results shown here. Minor adjustments to calibration may result in reduced AOD bias in the future, as was seen for SNPP VIIRS (Lyapustin et al., 2023), and this may be the best option for improving the UAA retrieval. Other options for improving the retrieval would include adjustments to the UAA aerosol models and wavelengths in the Look Up Tables and deriving a Machine Learning extrapolation to determine UV AOD over ocean.

The UAA applied to OCI is designed to be a work horse algorithm representing the global aerosol system with minimal global bias. All of these innovations: wide spectrum AOD, global quantification of SSA, aerosol layer height, AOD above clouds and 1-km resolution of the UVAI will enhance the PACE mission with daily, more comprehensive views of the global aerosol system, continuing day after day to build long term statistics and provide new insights on this key climate parameter on our changing planet.

Appendix A

The UAA produces two Level 2 output files, one at native resolution of the OCI, nominally 1 km, and the other in 7x7 grid boxes, nominally 7 km. The 1 km holds only a fine resolution Ultra Violet Aerosol Index (UVAI) as defined by Eq. 3, plus geolocation data and some diagnostics. This is file PACE/OCI/L2/UVAI_UAA/3.1 for Version 3.1. The 7 km product

https://doi.org/10.5194/egusphere-2026-3731
Preprint. Discussion started: 25 August 2026

holds all of the other parameters plus their geolocation, geometry, diagnostics and quality flags. This is file PACE/OCI/L2/AER_UAA/3.1.

The parameter lists are given in Tables A1 and A2.

Table A1. *Parameter list for nominal 1 km by 1 km file PACE/OCI/L2/UVAI_UAA/3.1* 1272 pixels per granule.

Group/Variable	Dimensions	Units	Notes
Geolocation Data			
longitude	(lines,pixels)	degrees	-180 ° to180 °
latitude	(lines,pixels)	degrees	-90 ° to 90 °
Geophysical_data			
NUV_AerosolIndex	(lines,pixels)	unitless	NUV Retrieved Aerosol Index (0.354-0.388 pair) at native 1km resolution
NUV_Residue	(lines,pixels)	unitless	NUV Retrieved LER based Aerosol Index (0.354-0.388 pair) at native 1km resolution
NUV_Reflectivity	(lines,pixels,2)	unitless	NUV Retrieved LERs for 0.354 and 0.388 µm, individually, at native 1km resolution

Table A2. *Parameter list for nominal 7 km by 7 km file PACE/OCI/L2/AER_UAA/3.1* 181 pixels per granule.

Group/Variable	Dimensions	Units	Notes
Geolocation Data			
longitude	(lines,pixels)	degrees	-180° to180 °
latitude	(lines,pixels)	degrees	-90 ° to 90 °
solar_zenith_angle	(lines,pixels)	degrees	0 ° to 180 °
solar_azimuth_angle	(lines,pixels)	degrees	-180 ° to180 °
sensor_zenith_angle	(lines,pixels)	degrees	0 ° to180 °
sensor_azimuth_angle	(lines,pixels)	degrees	-180 ° to180 °
Geophysical_data			
Land_Sea_Flag	(lines,pixels)	unitless	Land_Sea_Flag (0 = Ocean, 1 = Land)
Aerosol_Optical_Depth	(lines,pixels,9)	unitless	AOD @ 0.354, 0.388, 0.490, 0.550, 0.673, 0.865, 1.24, 1.61 and 2.25 µm

https://doi.org/10.5194/egusphere-2026-3731
Preprint. Discussion started: 25 August 2026

Optical_Depth_Ratio_Small_Ocean_used	(lines,pixels)	unitless	Fraction of AOD (at 0.55 micron) contributed by fine mode
Mean_Gas_Corrected_Reflectance	(lines,pixels,7)	unitless	Mean reflectance Gas corrected of pixels at 0.490, 0.550, 0.673, 0.865, 1.24, 1.61 and 2.25 µm
Mean_Reflectance	(lines,pixels,2)	unitless	Mean reflectance (not corrected for GAS) pixels at 0.354 0.388 µm
DT_AerosolSingleScattAlbedo	(lines,pixels,3)	unitless	Single scattering Albedo from Dark Target ocean subroutine at 0.354, 0.388 and 0.550 µm
DT_AerosolLayerHeight	(lines,pixels)	km	DDT Retrieved Aerosol Layer Height (1.5, 3, 6, 10 km). DIAGNOSIC. Use NUV_AerosolLayerHeight for science applications
Aerosol_Cld_Fraction_Land_Ocean	(lines,pixels)	unitless	DIAGNOSTIC
NUV_AerosolIndex	(lines,pixels)	unitless	NUV Aerosol Index (0.354-0.388 pair) at 7 km x7 km resolution
NUV_AerosolLayerHeight	(lines,pixels)	km	In km
NUV_AerosolSingleScattAlbedo	(lines,pixels,5)	unitless	NUV Retrieved Aerosol Single Scattering Albedo at 0.354, 0.388, 0.490, 0.550, 0.673 micron
NUV_RadiativeCloudFraction	(lines,pixels)	unitless	DIAGNOSTIC. NUV derived Radiative Equivalent Cloud Fraction at 0.388 µm
NUV_Residue	(lines,pixels)	unitless	DIAGNOSTIC
NUV_Reflectivity	(lines,pixels,2)	unitless	NUV Lambertian Equivalent Reflectivity (LER) at 0.354 and 0.388 µm
NUV_CloudOpticalDepth	(lines,pixels)	unitless	NUV Retrieved Cloud Optical Depth at 0.388 µm
NUV_AerosolOpticalDepthOverCloud	(lines,pixels,3)	unitless	NUV Retrieved Aerosol Optical Depth Over Cloud at 0.354, 0.388, 0.550 µm
NUV_AerosolCorrCloudOpticalDepth	(lines,pixels)	unitless	NUV Retrieved Aerosol Corrected Cloud Optical Depth at 0.388 µm

https://doi.org/10.5194/egusphere-2026-3731
Preprint. Discussion started: 25 August 2026

NUV_AerosolOpticalDepthOverCloudVsHeight	(lines,pixels,3,5)	unitless	NUV Retrieved Aerosol Optical Depth Over Cloud for 0.354, 0.388, 0.550 micron at 5 levels (3, 6, 9, 12, 15 km)
NUV_AerosolCorrCloudOpticalDepthVsHeight	(lines,pixels,5)	unitless	NUV Retrieved Aerosol Corrected Cloud Optical Depth for 0.388 micron at 5 levels (3, 6, 9, 12, 15 km)
NUV_FinalAlgorithmFlagsACA	(lines,pixels)	unitless	NUV Final Algorithm Flags for Above-cloud retrievals
NUV_UncertaintyACAODToSSA	(lines,pixels,2)	unitless	NUV derived percent uncertainty in COD due to change in SSA
NUV_UncertaintyCODToSSA	(lines,pixels,2)	unitless	NUV derived percent uncertainty in Aerosol-corrected COD due to plus/minus 0.03 change in SSA
Quality_flag_Aerosol_Optical_Depth	(lines,pixels)	unitless	Land=0 Ocean=0,1,2,3
Quality_flag_SingleScattAlbedo	(lines,pixels)	unitless	Quality_flag_SingleScattAlbedo 0,1,2,3
O2B_AerosolLayerHeight	(lines,pixels)	km	O2-B Retrieved Aerosol Layer Height

Code Availability: The Unified Aerosol Algorithm is open source code that can be found in the GitHub repository at: https://github.com/wingsy1212/PACE_OCI_unified_aerosol_retrieval_algorithm

Data Availability:

The PACI OCI Level-1B data that serves as input to the UAA is open access and publicly available. Version 3 was used to create the UAA products shown here.

NASA Ocean Biology Processing Group. (2024). *PACE OCI Level-1B Science Data, version 3* [Data set]. NASA Ocean Biology Distributed Active Archive Center. https://doi.org/10.5067/PACE/OCI/L1B/SCI/3 Date Accessed: 2025-12-23

https://doi.org/10.5194/egusphere-2026-3731
Preprint. Discussion started: 25 August 2026

The UAA 1-km UVAI is open access and publicly available
NASA Goddard Space Flight Center, Ocean Ecology Laboratory, Ocean Biology Processing Group. Ocean Color Instrument Level-2 UVAI_UAA,; NASA OB. DAAC, Greenbelt, MD, USA. doi:10.5067/PACE/OCI/L2/UVAI_UAA/3.1.

All other UAA products are open access and publicly available
NASA Goddard Space Flight Center, Ocean Ecology Laboratory, Ocean Biology Processing Group. Ocean Color Instrument Level-2 AER_UAA; NASA OB. DAAC, Greenbelt, MD, USA. doi:10.5067/PACE/OCI/L2/AER_UAA/3.1.

Author contribution:

Conceptualization	Remer, Torres, Hsu, Levy
Data curation	Jethva, Kayetha, Kim, Shi, Mattoo
Formal analysis	Shi, Jethva
Funding acquisition	Remer, Torres, Hsu, Levy
Investigation	Jethva, Remer, Torres, Kim, Kayetha, Shi, Mattoo, Levy, Hsu, Lee
Methodology	Mattoo, Remer, Torres, Hsu, Levy, Jethva, Kim, Kayetha, Shi, Lee
Project administration	Remer, Torres, Hsu, Levy
Software	Mattoo, Kayetha, Kim, Jethva, Shi, Lee
Supervision	Remer, Torres, Hsu, Levy
Validation	Shi, Jethva, Kim, Torres, Remer
Visualization	Jethva, Shi, Kim, Remer
Writing (original draft preparation)	Remer, Jethva, Kim
Writing (review and editing)	Levy, Kim, Torres, Jethva, Lee, Remer

https://doi.org/10.5194/egusphere-2026-3731
Preprint. Discussion started: 25 August 2026

Competing Interests: At least one of the (co-)authors is a member of the editorial board of Atmospheric Measurement Techniques.

Acknowledgements: The authors wish to thank the entire NASA PACE Project, the Ocean Biology Processing Group, the several iterations of the PACE Science and Applications Team and the hundreds of individuals who have made the PACE mission a reality and success. In particular, we acknowledge the leadership of Paula Bontempi, Laura Lorenzoni, Hal Maring, Mark Voyton, Juli Lander, Gary Davis, Bryan Franz, Gerherd Meister, Jeremy Werdell, Antonio Mannino, Brian Cairns, Emmanuel Boss and Heidi Dierssen. We also wish to thank NASA's AERONET team and the hundreds of AERONET PIs and site managers who maintain an unprecedented data base for satellite aerosol product validation. Finally, we recognize the effort of Andrew Sayer who will steward the UAA into the future.

Financial report: NASA grants NNX15AD15G and 80NSSC20M0209 provided the funding for the work.

References

Cohen, A.J., Brauer, M., Burnett, R., Anderson, H.R., Frostad, J., Estep, K., Balakrishnan, K., Brunekreef, B., Dandona, L., Dandona, R. and Feigin, V: Estimates and 25-year trends of the global burden of disease attributable to ambient air pollution: an analysis of data from the Global Burden of Diseases Study 2015. The lancet, *389*(10082), 1907-1918, doi:10.1016/S0140-6736(17)30505-6, 2017.

Eck, T. F., Holben, B. N., Reid, J. S., Dubovik, O., Smirnov, A., O'Neill, N. T., Slutsker, I., and Kinne,S.: Wavelength dependence of the optical depth of biomass burning, urban, and desert dust aerosols, J. Geophys. Res., 104(D24), 31333–31349, doi: https://doi.org/10.1029/1999JD900923, 1999.

Fraser, R. S., and Kaufman, Y.J.: The relative importance of aerosol scattering and absorption in remote sensing, *IEEE Trans. Geosci. Rem. Sens.* GE-23(5), 625-633, 10.1109/TGRS.1985.289380, 1985.

Giles, D. M., Sinyuk, A., Sorokin, M. G., Schafer, J. S., Smirnov, A., Slutsker, I., Eck, T. F., Holben, B. N., Lewis, J. R., Campbell, J. R., Welton, E. J., Korkin, S. V., and Lyapustin, A. I. (2019): Advancements in the Aerosol Robotic Network (AERONET) Version 3 database – automated near-real-time quality control algorithm with improved cloud screening for Sun

https://doi.org/10.5194/egusphere-2026-3731
Preprint. Discussion started: 25 August 2026

photometer aerosol optical depth (AOD) measurements, Atmos. Meas. Tech., **12**, 169-209, https://doi.org/10.5194/amt-12-169-2019.

Hashimoto, M. and Shi, C.: GOSAT-2 TANSO-CAI-2 L2 Pre-processing Algorithm Theoretical Basis Document-ATBD,NIES-GOSAT2-ALG-20191008-008-01, https://prdct.gosat-2.nies.go.jp/documents/pdf/ATBD_CAI-2_L2_C2PR_en_01.pdf (last access: 25 June 2023), 2020.

Herman, J. R., Bhartia, P. K., Torres, O., Hsu, C., Seftor, C., and Celarier, E.: Global distribution of UV-absorbing aerosols from Nimbus 7/TOMS data, J. Geophys. Res., 102(D14), 16911–16922, doi: https://doi.org/10.1029/96JD03680, 1997.

Holben B.N., T.F.Eck, I.Slutsker, D.Tanre, J.P.Buis, A.Setzer, E.Vermote, J.A.Reagan, Y.Kaufman, T.Nakajima, F.Lavenu, I.Jankowiak, and A.Smirnov, 1998: AERONET - A federated instrument network and data archive for aerosol characterization, *Rem. Sens. Environ.,* **66**, 1-16.

Hsu, N. C., Herman, J.R. and Tsay, S.C.: Radiative impacts from biomass burning in the presence of clouds during boreal spring in southeast Asia, *Geophys. Res. Lett.*, 30, 1224, doi:10.1029/2002GL016485, 5, 2003.

Hsu, N. C., Jeong, M.-J., Bettenhausen, C., Sayer, A.M., Hansell, R., Seftor, C. S., Huang, J., and Tsay, S.-C.: Enhanced Deep Blue aerosol retrieval algorithm: The second generation, *J. Geophys. Res. Atmos.*, 118, 9296–9315, doi:10.1002/jgrd.50712, 2013.

Hsu, N.C., Lee, J., Sayer, A.M., Kim, W., Bettenhausen, C. and Tsay, S.: VIIRS Deep Blue Aerosol Products Over Land: Extending the EOS Long-Term Aerosol Data Records, J. Geophys. Res., 124, 4026-4053, doi:10.1029/2018JD029688, 2019.

Ichoku, C., Chu, D.A., Mattoo, S., Kaufman, Y.J., Remer, L.A., Tanré, D., Slutsker, I. and Holben, B.N., A spatio-temporal approach for global validation and analysis of MODIS aerosol products, *Geophys. Res. Lett.*, 29(12), doi:10.1029/2001GL013206, 2002.

Jethva, H. and Torres, O.: Satellite-based evidence of wavelength-dependent aerosol absorption in biomass burning smoke inferred from Ozone Monitoring Instrument, Atmos. Chem. Phys., 11, 10541–10551, doi: https://doi.org/10.5194/acp-11-10541-2011, 2011.

Jethva, H., Torres, O., Remer, L. A., and Bhartia, P. K.: A Color Ratio Method for Simultaneous Retrieval of Aerosol and Cloud Optical Thickness of Above-Cloud Absorbing Aerosols From Passive Sensors: Application to MODIS Measurements, IEEE T. Geosci. Remote Sens., 51, 3862–3870, doi: https://doi.org/10.1109/TGRS.2012.2230008, 2013.

Jethva, H., O. Torres, and C. Ahn (2014), Global assessment of OMI aerosol single-scattering albedo using ground-based AERONET inversion, J. Geophys. Res. Atmos., 119, doi:10.1002/2014JD021672.

https://doi.org/10.5194/egusphere-2026-3731
Preprint. Discussion started: 25 August 2026

Jethva, H., Torres, O., and Ahn, C.: A 12-year long global record of optical depth of absorbing aerosols above the clouds derived from the OMI/OMACA algorithm, Atmos. Meas. Tech., 11, 5837–5864, doi: https://doi.org/10.5194/amt-11-5837-2018, 2018.

Kayetha, V., Torres, O., and Jethva, H.: Retrieval of UV–visible aerosol absorption using AERONET and OMI–MODIS synergy: spatial and temporal variability across major aerosol environments, Atmos. Meas. Tech., 15, 845–877, https://doi.org/10.5194/amt-15-845-2022, 2022.

Levy, R. C., Mattoo, S., Munchak, L. A., Remer, L. A., Sayer, A. M., Patadia, F., and Hsu, N. C.: The Collection 6 MODIS aerosol products over land and ocean, Atmos. Meas. Tech., 6, 2989–3034, doi: https://doi.org/10.5194/amt-6-2989-2013, 2013.

Lyapustin, A., Wang, Y., Choi, M., Xiong, X., Angal, A., Wu, A., Doelling, D.R., Bhatt, R., Go, S., Korkin, S. and Franz, B.: Calibration of the SNPP and NOAA 20 VIIRS sensors for continuity of the MODIS climate data records. Rem. Sens. of Environ., 295, 113717, 10.1016/j.rse.2023.113717, 2023

Marshak, A., Herman, J., Szabo, A., Blank, K., Cede, A., Carn, S., et al. (2018). Earth observations from DSCOVR EPIC instrument. Bull. Am. Meteorol. Soc. 99, 1829–1850, doi:10.1175/BAMS-D-17-0223.1

Martins, J. V., Tanré, D., Remer, L., Kaufman, Y., Mattoo, S. and Levy, R.: MODIS Cloud screening for remote sensing of aerosols over oceans using spatial variability, *Geophys. Res. Lett.*, 29(12), doi:10.1029/2001GL013252, 2002.

Meister,G.: OCI Spectral Response Tables. https://oceancolor.gsfc.nasa.gov/data/pace/characterization/. 2023. Last accessed 17 June 2026.

Meister, G. et al.: The Ocean Color Instrument (OCI) on the Plankton, Aerosol, Cloud, ocean Ecosystem (PACE) Mission: System Design and Prelaunch Radiometric Performance, IEEE Transactions on Geoscience and Remote Sensing, 62, 1-18, 5517418, doi: https://doi.org/10.1109/TGRS.2024.3383812, 2024.

Meyer, K., Platnick, S., and Zhang, Z.: Simultaneously inferring above-cloud absorbing aerosol optical thickness and underlying liquid phase cloud optical and microphysical properties using MODIS, J. Geophys. Res.-Atmos., 120, 5524–5547, doi: https://doi.org/10.1002/2015JD023128, 2015.

Remer, L. A., Kaufman, Y. J., Tanré, D., Mattoo, S., Chu, D. A., Martins, J. V., Li, R.-R., Ichoku, C., Levy, R. C., Kleidman, R. G., Eck, T. F., Vermote, E., and Holben, B. N.: The MODIS aerosol algorithm, products and validation. J. Atmos. Sci., 62, 947-973, doi: https://doi.org/10.1175/JAS3385.1, 2005.

Remer, L. A., Mattoo, S., Levy, R. C., Heidinger, A., Pierce, R. B., and Chin, M.: Retrieving aerosol in a cloudy environment: aerosol product availability as a function of spatial resolution, Atmos. Meas. Tech., 5, 1823–1840, https://doi.org/10.5194/amt-5-1823-2012, 2012.

https://doi.org/10.5194/egusphere-2026-3731
Preprint. Discussion started: 25 August 2026

Remer L. A., R. C. Levy, S. Mattoo, Tanré, D., Gupta, P., Shi, Y.R., Sawyer, V., Munchak, L.A., Zhou, Y., Kim, M., Ichoku, C., Patadia, F., Li, R.-R., Gassó, S., Kleidman, R.G. and Holben, B.N.: The Dark Target Algorithm for Observing the Global Aerosol System: Past, Present, and Future. *Remote Sensing* **12 (18)** 2900 doi:10.3390/rs12182900, 2020.

Satheesh, S. K., Torres, O., Remer, L. A., Babu, S. S., Vinoj, V., Eck, T. F., Kleidman, R. G., and Holben, B. N.: Improved assessment of aerosol absorption using OMI-MODIS joint retrieval, J. Geophys. Res., 114, D05209, doi: https://doi.org/10.1029/2008JD011024, 2009.

Satheesh, S. K., Vinoj, V., and Krishnamoorthy, K., Assessment of aerosol radiative impact over oceanic regions adjacent to Indian subcontinent using multi-satellite analysis, Hindawi Publishing Corporation, Advances in Meteorology, Volume 2010, Article ID 139186, doi:10.1155/2010/139186

Sawyer, V., Levy, R., Mattoo, S., Cureton, G. Shi, Y. Remer, L.A.: Continuing the MODIS Dark Target aerosol time series with VIIRS, Remote Sens. 12, 308, doi: https://doi.org/10.3390/rs12020308, 2020.

Sawyer, V., Levy, R.C., Mattoo, S., Shi, Y.R., Kim, M., Remer, L.A. and Cureton, G.:An updated VIIRS dark target aerosol product for continuity with MODIS: assessing regional aerosol trends. Front. Environ. Sci., 13, doi.org/10.3389/fenvs.2025.1602145, 2025.

Sayer, A. M., Munchak, L. A., Hsu, N. C., Levy, R. C., Bettenhausen, C., and Jeong, M.-J.: MODIS Collection 6 Aerosol Products: Comparison between Aqua's E-Deep Blue, Dark Target, and "Merged" Data Sets, and Usage Recommendations. Journal of Geophysical Research Atmosphere, 119, 13,965-13,989, doi: https://doi.org/10.1002/2014JD022453, 2014.

Sayer, A. M., Hsu, N. C., Bettenhausen, C., Lee, J., Redemann, J., Schmid, B., and Shinozuka, Y.: Extending "Deep Blue" aerosol retrieval coverage to cases of absorbing aerosols above clouds: Sensitivity analysis and first case studies, J. Geophys. Res. Atmos., 121, doi: https://doi.org/10.1002/2015JD024729, 2016.

Sayer, A. M., Govaerts, Y., Kolmonen, P., Lipponen, A., Luffarelli, M., Mielonen, T., Patadia, F., Popp, T., Povey, A. C., Stebel, K., and Witek, M. L.: A review and framework for the evaluation of pixel-level uncertainty estimates in satellite aerosol remote sensing, Atmos. Meas. Tech., 13, 373–404, https://doi.org/10.5194/amt-13-373-2020, 2020.

Smirnov, A., Holben, B.N., Slutsker, I., Giles, D.M., McClain, C.R., Eck, T.F., Sakerin, S.M., Macke, A., Croot, P., Zibordi, G., Quinn, P.K., Sciare, I., Kinne, S., Harvey, M., Smyth, T.J., Piketh, S., Zielinski, T., Proshutinsky, A., Goes, J.I., Nelson, N.B., Larouche, P. Radionov, V.F., Goloub, P., Krishna Moorthy, K., Matarrese, R., Robertson, E.F., Jourdin, F.: Maritime Aerosol Network as a component of Aerosol Robotic Network, *J. Geophys. Res.*, 114, D06204, doi:10.1029/2008JD011257, 2009.

Szopa, S., Naik, V., Adhikary, B., Artaxo, P., Berntsen, T., Collins, W.D., Fuzzi, S., Gallardo, L., Kiendler-Scharr, A., Klimont, Z., Liao, H., Unger, N., & Zanis, P.: *Short-Lived Climate Forcers (Chapter 6).* In: IPCC 2021: Climate Change 2021: The Physical Science Basis. Contribution of Working Group I to the Sixth Assessment Report of the Intergovernmental Panel

https://doi.org/10.5194/egusphere-2026-3731
Preprint. Discussion started: 25 August 2026

on Climate Change. Eds. Masson-Delmotte, V., Zhai, P., Pirani, A., Connors, S.L., Péan, C., Berger, S., Caud, N., Chen, Y., et al., pp. 817-922 Cambridge, United Kingdom and New York, NY, USA: Cambridge University Press.10.1017/9781009157896.008, 2021.

Torres, O., Bhartia, P. K., Herman, J. R., Ahmad, Z., and Gleason, J.: Derivation of aerosol properties from satellite measurements of backscattered ultraviolet radiation: Theoretical basis, J. Geophys. Res., 103(D14), 17099–17110, doi: https://doi.org/10.1029/98JD00900, 1998.

Torres, O., P. K. Bhartia, A. Sinyuk, E. J. Welton, and B. Holben: Total Ozone Mapping Spectrometer measurements of aerosol absorption from space: Comparison to SAFARI 2000 ground-based observations, J. Geophys. Res., 110, D10S18, doi:10.1029/2004JD004611, 2005.

Torres, O., Tanskanen, A., Veihelmann, B., Ahn, C., Braak, R., Bhartia, P. K., Veefkind, P., and Levelt, P.: Aerosols and surface UV products from Ozone Monitoring Instrument observations: An overview, J. Geophys. Res., 112, D24S47, doi: https://doi.org/10.1029/2007JD008809, 2007.

Torres, O., Jethva, H., and Bhartia, P. K.: Retrieval of Aerosol Optical Depth above Clouds from OMI Observations: Sensitivity Analysis and Case Studies, J. Atmos. Sci., 69, 1037-1053, doi: https://doi.org/10.1175/JAS-D-11-0130.1, 2012.

Torres, O., Ahn, C., and Chen, Z.: Improvements to the OMI near-UV aerosol algorithm using A-train CALIOP and AIRS observations, Atmos. Meas. Tech., 6, 3257–3270, https://doi.org/10.5194/amt-6-3257-2013, 2013.

Torres, O., Remer, L.A.: History of passive remote sensing of aerosol from space. In: Lenoble, J., Remer, L., Tanre, D. (eds) Aerosol Remote Sensing. Springer, Berlin, Heidelberg. https://doi.org/10.1007/978-3-642-17725-5_7, 2013

Torres, O., Jethva, H., Ahn, C., Jaross, G., and Loyola, D. G.: TROPOMI aerosol products: evaluation and observations of synoptic-scale carbonaceous aerosol plumes during 2018–2020, Atmos. Meas. Tech., 13, 6789–6806, https://doi.org/10.5194/amt-13-6789-2020, 2020.

Torres O, Jethva H, Ahn C and Kayetha V.: A decade of global hourly aerosol observations from DSCOVR/EPIC using near-UV measurements, Front. Remote Sens. 6:1685415. doi: 10.3389/frsen.2025.1685415, 2025

Werdell, P. J., and Coauthors: The Plankton, Aerosol, Cloud, Ocean Ecosystem Mission: Status, Science, Advances. Bull. Amer. Meteor. Soc., 100, 1775-1794, doi: https://doi.org/10.1175/BAMS-D-18-0056.1, 2019.

Xu, X., Wang, J., Wang, Y., Zeng, J., Torres, O., Yang, Y., Marshak, A., Reid, J., and Miller, S.: Passive remote sensing of altitude and optical depth of dust plumes using the oxygen A and B bands: First results from EPIC/DSCOVR at Lagrange-1 point, Geophys. Res. Lett., 44, 7544-7554, doi: https://doi.org/10.1002/2017GL073939, 2017.

Xu, X., Wang, J., Wang, Y., Zeng, J., Torres, O., Reid, J. S., Miller, S. D., Martins, J. V., and Remer, L. A.: Detecting layer height of smoke aerosols over vegetated land and water surfaces via

https://doi.org/10.5194/egusphere-2026-3731
Preprint. Discussion started: 25 August 2026

oxygen absorption bands: hourly results from EPIC/DSCOVR in deep space, Atmos. Meas. Tech., 12, 3269-3288, doi: https://doi.org/10.5194/amt-12-3269-2019, 2019.

Yu, H., Remer, L.A., Chin, M., Bian, H., Kleidman, R.G. and Diehl, T.: A satellite-based assessment of transpacific transport of pollution aerosol. J. Geophys. Res.: Atmos., *113*(D14), doi: 10.1029/2007JD009349, 2008.

Yu, H., Remer, L.A., Chin, M., Bian, H., Tan, Q., Yuan, T. and Zhang, Y.: Aerosols from overseas rival domestic emissions over North America. Science, *337*, 566-569, DOI: 10.1126/science.121757, 2012.

Yu, H., Remer, L.A., Kahn, R.A., Chin, M. and Zhang, Y.:Satellite perspective of aerosol intercontinental transport: From qualitative tracking to quantitative characterization. Atmos. Res., 124, 73-100, doi:10.1016/j.atmosres.2012.12.013, 2013.